SANDIA REPORT

SAND2012-10608
Unlimited Release
Printed December 2012

Enhanced Micellar Catalysis LDRD

Rita G. Betty, Crystal Glen, Todd Alam, Gretchen Taggart, Danielle Rivera, Mark Kinnan, and Mark Tucker

Prepared by
Sandia National Laboratories
Albuquerque, New Mexico 87185 and Livermore, California 94550

Sandia National Laboratories is a multi-program laboratory managed and operated by Sandia Corporation, a wholly owned subsidiary of Lockheed Martin Corporation, for the U.S. Department of Energy's National Nuclear Security Administration under contract DE-AC04-94AL85000.

Issued by Sandia National Laboratories, operated for the United States Department of Energy by Sandia Corporation.

Available to DOE and DOE contractors from
U.S. Department of Energy
Office of Scientific and Technical Information
P.O. Box 62
Oak Ridge, TN 37831

Telephone: (865) 576-8401
Facsimile: (865) 576-5728
E-Mail: reports@adonis.osti.gov
Online ordering: http://www.osti.gov/bridge

Available to the public from
U.S. Department of Commerce
National Technical Information Service
5285 Port Royal Rd.
Springfield, VA 22161

Telephone: (800) 553-6847
Facsimile: (703) 605-6900
E-Mail: orders@ntis.fedworld.gov
Online order: http://www.ntis.gov/help/ordermethods.asp?loc=7-4-0#online

SAND2012-10608
Unlimited Release
Published December 2012

Enhanced Micellar Catalysis LDRD

Rita G. Betty, Mark Tucker, Gretchen Taggart, and Mark Kinnan
Chemical and Biological Systems Department, 06632
Sandia National Laboratories
P.O. Box 5800
Albuquerque, New Mexico 87185-0734

Crystal Glen, Danielle Rivera, and Andres Sanchez
Fire Aerosol and Sciences Department, 01532
Sandia National Laboratories
P.O. Box 5800
Albuquerque, New Mexico 87185-1135

Todd Alam
Electronic and Nanostructured Materials, 01816
Sandia National Laboratories
P.O. Box 5800
Albuquerque, New Mexico 87185-0886

Abstract

The primary goals of the Enhanced Micellar Catalysis project were to gain an understanding of the micellar environment of DF-200, or similar liquid CBW surfactant-based decontaminants, as well as characterize the aerosolized DF-200 droplet distribution and droplet chemistry under baseline ITW rotary atomization conditions. Micellar characterization of limited surfactant solutions was performed externally through the collection and measurement of Small Angle X-Ray Scattering (SAXS) images and Cryo-Transmission Electron Microscopy (cryo-TEM) images. Micellar characterization was performed externally at the University of Minnesota's Characterization Facility Center, and at the Argonne National Laboratory Advanced Photon Source facility. A micellar diffusion study was conducted internally at Sandia to measure diffusion constants of surfactants over a concentration range, to estimate the effective micelle diameter, to determine the impact of individual components to the micellar environment in solution, and the impact of combined components to surfactant phase behavior. Aerosolized DF-200 sprays were characterized for particle size and distribution and limited chemical composition. Evaporation rates of aerosolized DF-200 sprays were estimated under a set of baseline ITW nozzle test system parameters.

ACKNOWLEDGMENTS

Sandia Contributors:

- Decontamination Chemistry – Rita G. Betty, Mark Tucker, Gretchen Taggart
- Nuclear Magnetic Resonance Analyses – Todd Alam
- Aerosol Science – Crystal Glen, Danielle Rivera, Andres Sanchez
- Dynamic Light Scattering Analyses – Mark Kinnan, Kevin Crown
- Small Angle Light Scattering – Hongyou Fan, Binsong Li

External Participants, Small Angle X-Ray Scattering:

- Soenke Seifert – Argonne Advanced Photon Source Facility
- Linda Sauer, Michael Manno, Robert Hafner – University of Minnesota Characterization Facility Center. Parts of this work were carried out in the Institute of Technology Characterization Facility, University of Minnesota, which receives partial support from NSF through the NNIN program.

Management Team: Duane Lindner, Bruce Kelley, Randy Watkins

CONTENTS

FIGURES

TABLES

1. INTRODUCTION

Sandia National Laboratories has been a leader in the development of decontamination technologies for use against chemical and biological warfare (CBW) agents, toxic industrial chemicals and other toxins for use in both the military and civilian arenas. The most widely known decontaminant, DF-200 was developed beginning in the late 1990's, licensed to two companies and is commercially available as "EasyDecon" (manufactured by EFT Holdings, Inc.) and "MDF-200" (manufactured by Modec, Inc.). The patented technology has been fielded by the U.S. Department of Defense internationally. DF-200 is an aqueous based tertiary mixture of cationic surfactants, select co-solvents, mild peroxide and bicarbonate salts. Once mixed on demand, the final reactive solution has been demonstrated to be highly effective in the neutralization of all classes of CBW agents for which it has been tested. For example, in tests conducted by the DOD, the DF-200 decontamination efficacies of HD, VX and G agents were determined to be > 99.8%, > 99.8%, and >99.9% following 30 minutes of contact exposure time on Chemical Agent Resistant Coating (CARC) coupons.

Success of the DF-200 technology was attained without the benefit of building from known fundamental key physical and chemical properties and conditions at the micellar and molecular level that impact decontamination performance. As an example of CW decontamination, the neutralization of G-agents occurs through nucleophilic substitution at the critical P-F bond. In the case of DF-200, the cleavage at this bond is enhanced by the presence of cationic micelles, which serve to attract and provide a nucleophilic-rich environment of the anionic species hydroxide, hydroperoxicarbonate, and hydroperoxide ions. The anionic species are produced by the breakdown of hydrogen peroxide, bicarbonate or carbonate salts, and peroxide activators such as ethylene glycol diacetate in aqueous solutions. Reaction rates in solution are rapid due to the availability and close proximity of the anionic reactive species to the chemical agents; the anionic nucleophiles rapidly cleave the P-F bond via the SN_2 nucleophilic substitution reaction. A diagram depicting the formation of the reactive anionic species in solution and cationic micellar catalysis is shown in Figure 1.

Figure 1. Micellar Catalysis in a Mixed Reactive System

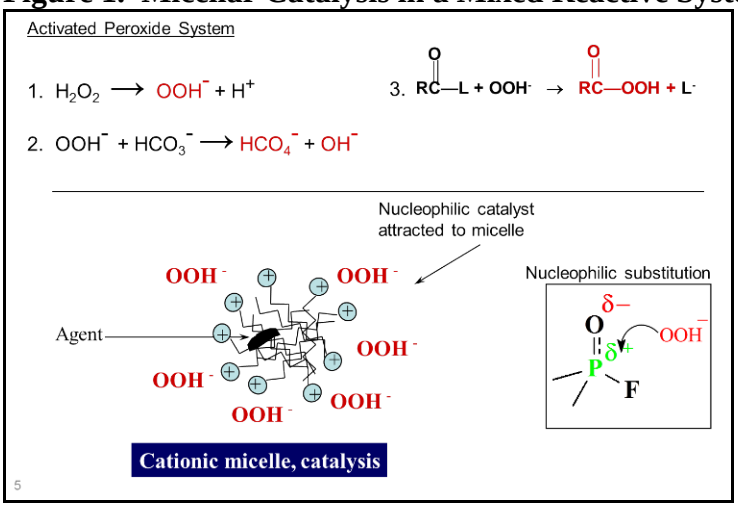

However, as the cause and effect of component addition to the micellar environment has not been studied on the micro scale, it is very highly likely that performance optimization has not yet been achieved. The goals of this LDRD project were to gain fundamental knowledge of cause and effect on micellar catalysis as key formulation components, both reactive and non-reactive, are combined to form effective micelle-based decontaminating liquids. Imaging techniques were used to collect micelle size and other physical attributes. Nuclear magnetic resonance techniques were used to further characterize micellar mixtures such as micelle size, and to monitor the diffusion of components into a micellar structure, or their presence free in the bulk liquid. Data collected under the micellar partition study can be compared to kinetics performance, to deduce how changes in the formulation chemistry impact performance. Thus, the correlation of micellar characterization to performance would ideally provide guidance for continued formulation development that could be used to meet sponsor directed objectives.

The characterization of aerosolized decontaminant droplet chemistry and evaporation rates (FY2012) of aerosolized particles and in the vapor phase will ultimately increase our knowledge of reactive species and effective concentrations in these environments. From the perspective of the CBRN mitigation response program, an ultimate goal is the ability to fine tune rotary atomization spray nozzle and system parameters based on threat characterization and the knowledge of aerosolized reactive species, their efficacies and residence time.

Once correlated to simulant and agent performance data, it is anticipated that the micellar characterization of effective and ineffective formulations will inform future development of application-specific decontaminants. Results may suggest formulation and/or deployment method modifications, optimizing the efficacy of micellar catalysis across broad use for neutralization of liquid, aerosolized particle or vaporous phases of contamination. Incorporation of enhanced micellar catalysis knowledge into current decontamination deployment methods will expand Sandia's expertise and capabilities in CBW decontamination technology.

The commercial and government customer base is broad and for many applications, already very well established. Potential customers and sponsors include DHS, military agencies (the Defense Threat Reduction Agency, and US Army Chemical Materials Agency), and public health and transportation industries.

2. MICELLAR CHARACTERIZATION

2.1. Initial Dynamic Light Scattering Techniques

Dynamic Light Scattering (DLS) - Dynamic light scattering measures the Brownian motion of molecules and particles in solution, from which size and size distributions may be determined. Dynamic and static light scattering techniques were used to analyze the size of micelles formed in solution. Three different instruments and techniques were used to attempt to acquire micelle size and characterization data: an R&D grade Brookhaven Instruments BI-200 SM; the Malvern Nano-ZsZetasizer (two separate units); and the Microtex Nanotrac Particle Size Analyzer PSA, a unit commonly used for industrial quality control purposes.

The composition of the micelle solutions analyzed for this study was based on the DF-200 CBW decontamination technology Part A (surfactant and co-solvent portion), and also on select surfactants that could be considered for test and evaluation under other decontamination formulation development efforts. Although an exhaustive effort was made to collect data, consistent information on micelle size could not be acquired for the surfactant solutions using these dynamic or static light scattering techniques. Effervescence from the breakdown of peroxide (concentrations 3-5%) in solution interfered with the light scattering process, as gas particles passed through the detector cells.

In parallel with the internal collection of DLS particle size data, Particle Technology Labs, an industry leader in particle analysis, was contacted to outsource analysis of select surfactant solutions for the determination of micelle size. The select surfactant solutions could not be analyzed for micelle size using light scattering techniques because of two factors: the viscosity of the solvent(s) was an order of magnitude too high for accurate micelle analysis; and the concentration of the surfactant in the solvent(s) was several orders of magnitude too high for determining micelle size. The recommendation of Particle Technology Labs was to perform cryogenic Transmission Electron Microscopy (cryo-TEM) as a possible option for obtaining the micelle size in solution. Through recommendation of a fellow Sandian, UMN Characterization Facility personnel were contacted to perform scoping SAXS and cryo-TEM analyses, discussed in Section 2.2.1 and 2.3.

2.1.1. Preliminary DLS Experimental Results - contributed by Mark Kinnan, Sandia National Laboratories

As explained previously, minimal data was obtained by dynamic light scattering techniques. Table 1 below is an overview of the measured particles sizes of Berol® 226 SA, a commercially available surfactant comprised of a proprietary quaternary amine compound (40-60% by weight), ethoxylated alcohol (40-60% by weight), and a diluent. The Berol product was evaluated as a potential surfactant constituent of developmental decontamination formulations for both homeland security and military applications.

Table 1. Overview of Particle Sizes - The * denotes the size of the majority of the particles.

Berol Concentration In Water	Software Calculated Diameter (nm)*	Manually Calculated Diameter (nm)*	Calculated Error*
0.1%	8.0	7.8	4%
0.01%	2.1	0.3	8%
0.001%	260.6	261.3	0.5%

Berol in Water

It was found for 0.1% Berol in water, approximately 8 nm diameter particles were observed. A few larger particles were observed as evident of the higher intensity scattering peaks, Figure 2. When the concentration of Berol in water was decreased to 0.01% there was a significant amount of scattering from larger particles in solution. The peaks observed in Figures 2a. and 2b. are broad which indicates large particles were in the path of the laser for an extended period of time. The larger intensity scattering peaks for 0.1% and 0.01% concentrations are attributed to phase separated particles of Berol instead of dust/dirt. In other words, the longer a particle is in the path of the laser the broader the scattered peak becomes. For comparison when a dust/dirt particle enters the path of laser, a scattering plot of a 20nm latex standard in water is presented in Figure 2d. It can be observed that when a dust/dirt particle enters the path of the laser, the result is a narrow scattered peak as compared to a broad peak.

Figure 2c. is the scattering plot for a 0.001% Berol in water solution. The solution was found to contain a monodisperse solution of 260 nm particles. Attempts were made to identify small (~ 10 nm) particles but none were observed.

The decrease in Berol from 0.01% to 0.001% resulted in 260 nm particles, an unexpected observation. One might speculate that the Berol solution is not miscible with water at lower concentrations because there are not enough stabilizer molecules (found in the Berol solution) to keep Berol solubilized. At higher concentrations of Berol in water the amount of stabilizers is high enough to keep Berol miscible with water to create smaller particles (e.g., micelles). As the concentration of Berol in water is decreased, the amount of stabilizer is also decreased which results in decreased miscibility of Berol in water. Therefore, the Berol remains in an ‘oil like’ phase in the form of oil droplets in water.

Figure 2. DLS Scattering Plots of Berol 226SA solutions in DI water

Figure 2a.

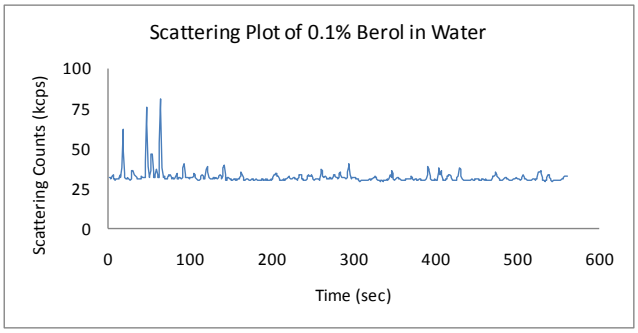

Figure 2b.

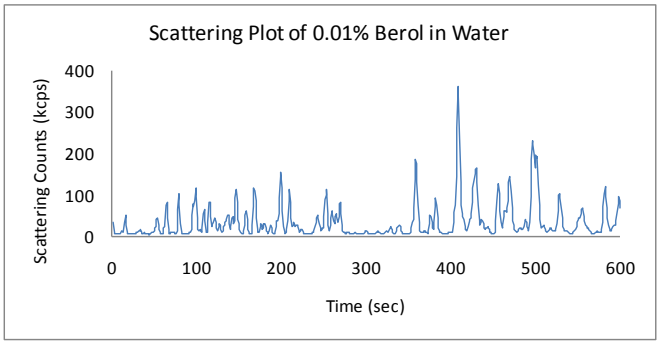

Figure 2c.

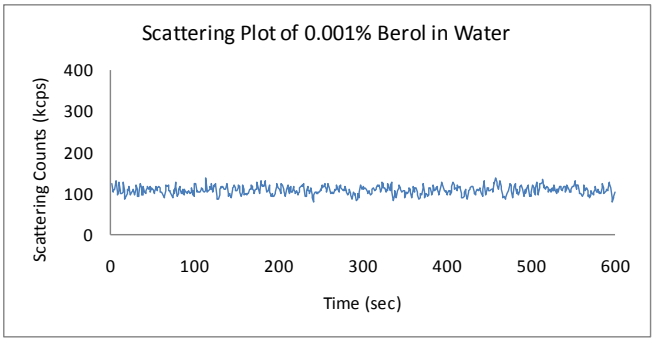

Figure 2d.

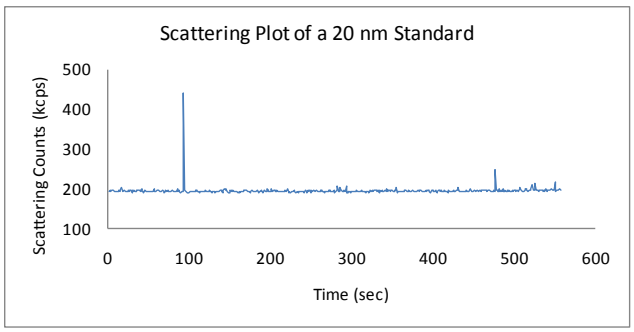

2.2. Small Angle Light Scattering

In addition to cryo-TEM, Small Angle Light Scattering (SAXS) analyses was sought to characterize micelles in solution. SAXS capability was pursued externally to Sandia National Laboratories, as the technique was not available internally at the time of this project. For a brief overview of SAXS methodology, refer to the publication authored by Aswal.

Several facilities with SAXS competency were identified and contacted. Two of the facilities, the University of Minnesota Characterization Facility and Argonne Advanced Photon Source expressed interest in collecting solution-based micelle characterization data. These independent efforts are described in the following sections.

2.2.1. University of Minnesota (UMN) – Institute of Technology Characterization Facility

The objective of the initial work performed by UMN was to characterize the micellar environment (size, shape, phase, etc.) observed within two different surfactant solutions comprised of 2% Variquat 80MC (a quaternary ammonium surfactant component of DF-200, Alkyl dimethylbenzyl ammonium chloride) in deionized water, or 2% Berol 226 SA (a proprietary blend of 40-60% ethoxylated alcohol, 40-60% quaternary amine 40-60%, and 10-20% diluent, manufactured by AkzoNobel) in Lumulse POE-12 (ethoxylated glycerine with approximately 12 moles of ethylene oxide). The alkyl chain of Variquat is comprised of 60% C14, 25% C12, and 15% C16 chain length. These initial tasks were performed to gain a greater certainty of the experimental techniques required for micellar characterization of these systems. The tasks included collection and measurement of SAXS images of various surfactant solutions, and all subsequent data analysis. A follow-on task was to perform micellar characterization of the EasyDecon reactive mixture. As observed in earlier efforts, the effervescence provided interference to the analysis.

Reports included appropriate SAXS image plates, integrated plots, background subtracted files, cryo-TEM images and full data analyses for the solution sets. All resultant L and Q scans were integrated with the same width (600 pixels), while ensuring a constant primary beam width. Detector images were scaled with a similar intensity contrast and maximum.

Methodology

Small-angle x-ray scattering was performed at the Characterization Facility of the University of Minnesota using the Anton Paar SAXSess instrument with copper radiation and image plate detectors. Power settings were 45 kV, 40 ma. The samples were prepared and the quartz capillary sample holder was used at room temperature. Data was collected for 1800 seconds per sample with water in the quartz capillary used as the background. Ten minute scans were collected, with the imaging plate notch oriented facing upward in both the machine and Cyclone. A minimum five minute bleaching of image plates was performed between scans. All resultant scattering intensity I vs. scattering vector Q (inverse nm) scans were integrated with the same width (600 pixels), while ensuring a constant primary beam width. Detector images were scaled with a similar intensity contrast and maximum. The two-dimensional P image plates were integrated to produce the one-dimensional plots of Scattering Intensity vs. Scattering Vector, Q (nm^{-1}). The relational equation to spacing distance is $Q = 4\pi/d$.

Results - Preliminary scoping effort – The initial tasks were performed to gain a greater certainty of the experimental techniques required for micellar characterization of two different surfactant solutions comprised of 2% Variquat 80MC in deionized water, or 2% Berol in Lumulse. Results indicated a broad Variquat peak centered at 9.3 nm. Analysis of the Berol sample was more challenging; completion of the analysis would require additional modeling by small angle software, or change in the solvent to produce a less viscous system. Additional analysis of the Berol was not pursued.

Figure 3. SAXS imaging and plot of Scattering Intensity vx Scattering Vector, Q for 2% Variquat in deionized water.

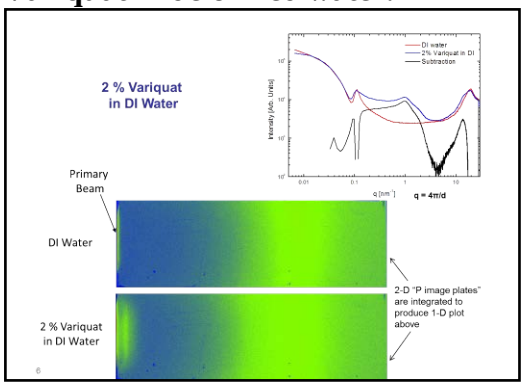

Figure 4. SAXS image plates and plot for 2% Berol in Lumulse

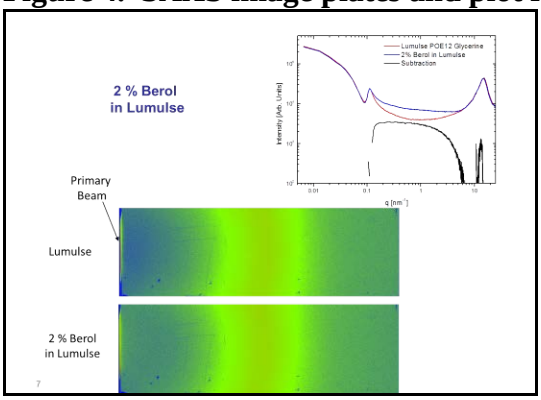

Figure 5. As shown in this figure, Small Angle X-ray scattering intensity, I, is a function of scattering vector $Q = 4\pi\sin\theta/\lambda$, where 2θ is the scattering angle and λ is the wavelength of incident radiation.

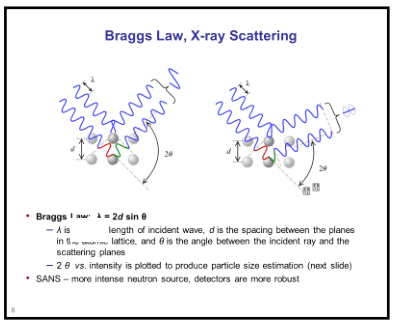

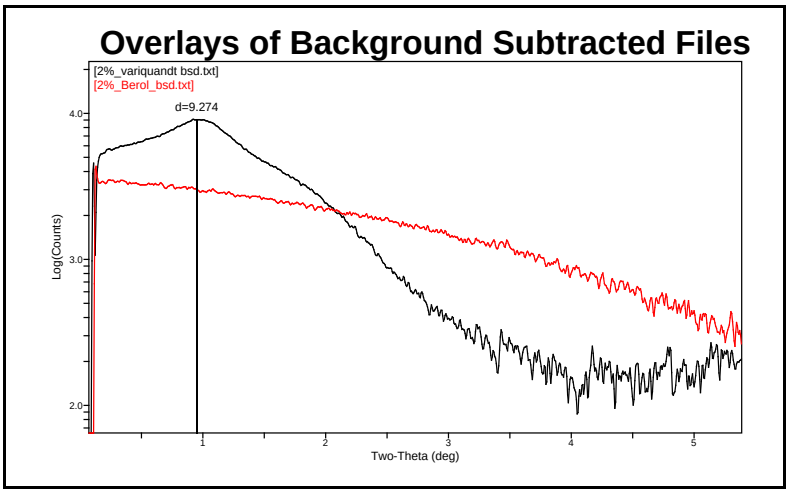

Figure 6. Background subtracted plots of 2% Variquat and 2% Berol solutions; the Log (Counts) response versus 2 Theta (deg), where $\lambda = 2d \sin\theta$

Preliminary SAXS data evaluating the micelle size distribution and shape of dilute Variquat 80MC (the primary quaternary ammonium surfactant in the DF-200 formulation) indicated spherical micelles over a broad size range, averaging around 9 nm. The preliminary cryo-TEM data suggested spherical micelles ranging from 15-25 nm. Further SAXS analyses may require alternate modeling approaches within the SAXS software, or evaluation of less viscous solutions. A contract was placed in May 2011 for UMN to perform additional SAXS and cryo-TEM analyses to determine micellar conditions of various surfactant blends.

The objective of the follow-in contract at UMN was to characterize the micellar environment (size, shape, phase, etc.) observed within the following surfactant solutions:

- EasyDecon (reactive), diluted solutions at ratios of 1:25, 1:250, 1:2500 in deionized water
- 2% Berol in deionized water (to compare w/ 2% Variquat in DI water data)

Results of the follow-on effort are described in the next section.

Results - Follow-on effort, UMN - Only Variquat 80MC showed any scattering different than the water background as illustrated in Figure 8 below. Because of the lack of scattering contrast and the small size of the Variquat 80MC structure, cryo TEM analysis of the Variquat 80MC was not recommended.

The scattering peak for Variquat 80MC and its shoulder at Q value of ~ 1 can be attributed either a bimodal sphere distribution or to a core shell structure with a mean value roughly around 16 Angstroms. From the Variquat 80MC MSDS, the structure has a head and tail, but the MSDS reports some polydispersity in the tail length which makes data fitting very difficult and problematic. An attempt was made to fit the data using IGOR (a NIST SAXS data fitting program) with little success, and results were inconclusive.

Figure 7. Overlays of SAXS scans (surfactants, EasyDecon, and deionized water background). The Intensities were normalized and include background subtraction.

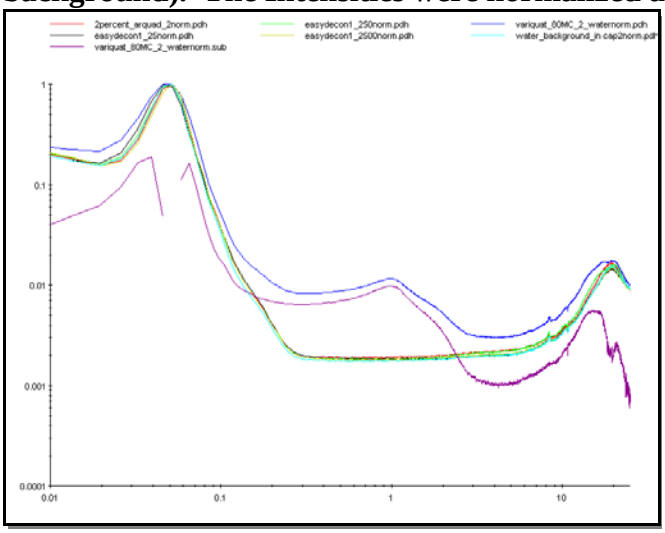

Figure 8. An expanded view of the lower q region, SAXS – Only the 2% Variquat 80MC solution exhibited scattering at low angles.

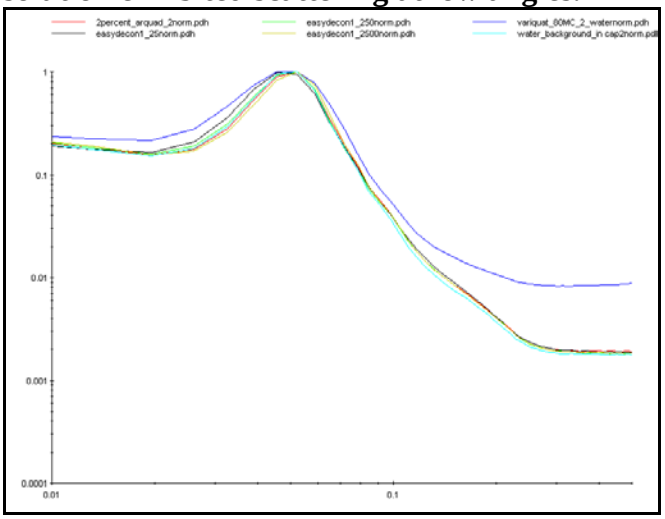

Figure 9. P Image Plates - Deionized water background, 2% Variquat, and EasyDecon 1:250 and 1:2500 dilutions. Of the test solutions, only the 2% Variquat sample demonstrated SAXS scattering.

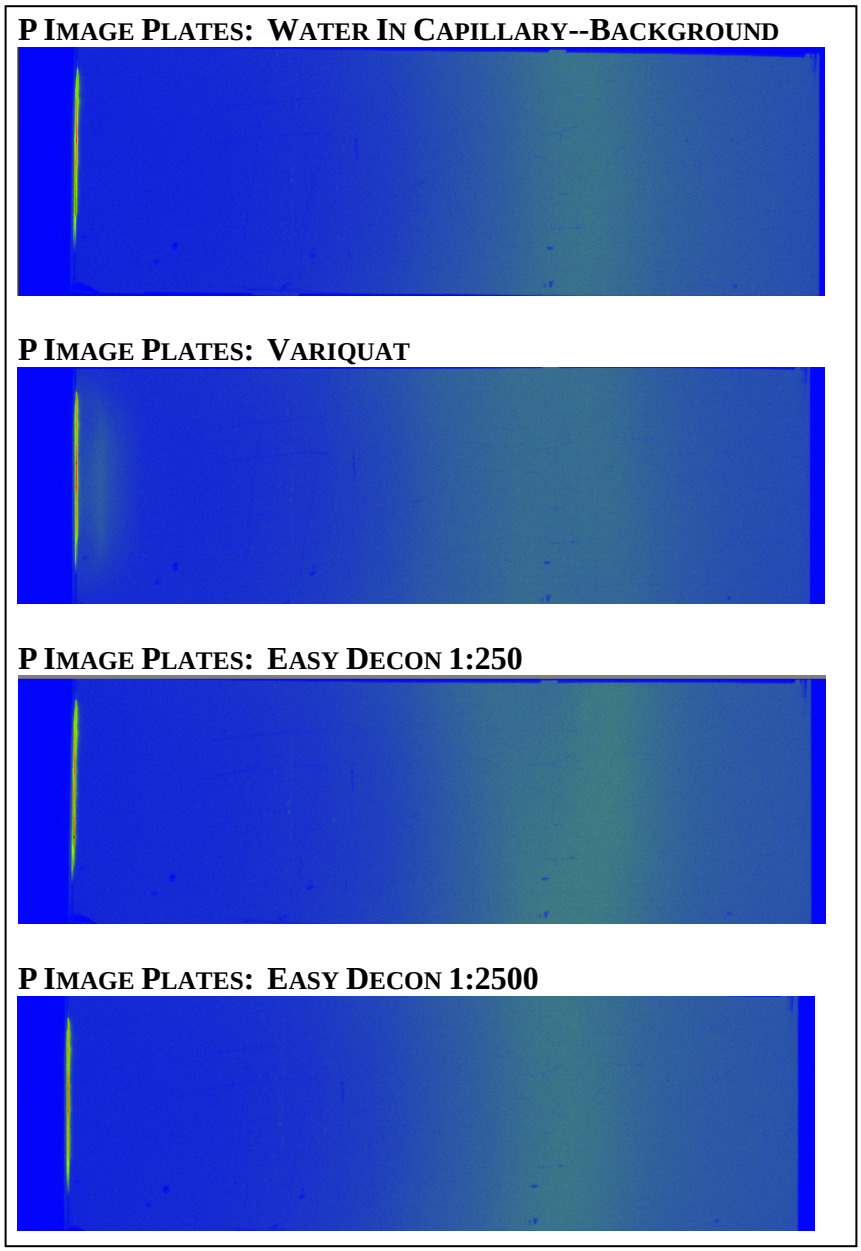

2.2.2. Cornell University – Cornell High Energy Synchrotron Source

The purpose of this study was to evaluate the micellar characteristics of surfactant solutions that may be considered for use as components in developmental decontaminants.

The following solutions were prepared for analyses:

1. 0.6105 weight % dodecyltrimethylammonium chloride (DTAC, CAS# 112-00-5), remainder deionized water

2. 0.0165 weight % N,N-dimethyl-1-dodecanamine (CAS# 112-18-5), remainder deionized water

3. 0.6105 wt% dodecyltrimethylammonium chloride
   0.0165 wt% N,N-dimethyl-1-dodecanamine, remainder deionized water

4. 0.6105 wt% dodecyltrimethylammonium chloride
   0.0165 wt% N,N-dimethyl-1-dodecanamine
   1.65 wt% propylene glycol (CAS# 57-55-6), remainder deionized water

Methodology

Grazing incidence small-angle X-ray scattering (GISAXS) measurements were performed on D1 station of the Cornell High Energy Synchrotron Source (CHESS). The X-ray beam was produced by a hard bend magnet HB5E and monochromatized with 30 Å Mo:B_4C multilayers. The X-ray energy was 10.6199 keV, corresponding to a wavelength of 1.1688 Å. The beam size was about 0.5 mm horizontally and 0.1 mm vertically. The beamline was equipped with a 2-D area detector (MedOptics CCD) with a pixel size of 46.9 μm by 46.9 μm and a total of 1024 x 1024 pixels. The sample to detector distance was 603.30 mm as determined by a silver behenate powder standard. The incident angle of the X-ray beam was 0.25°, and images were taken with an exposure time of 5 s. GISAXS images were calibrated and integrated using the Fit2D software.

Results – contributed by Binsong Li and Hongyou Fan, Sandia National Laboratories

GISAXS analyses were performed on surfactant solutions at the Cornell University facility. No peaks were detected in the surfactant solutions. The solutions were also applied as droplets on silicon wafers, and allowed to evaporate overnight to dry film formation. GISAXS images and analyses were then performed on the dried films. These results were inclusive; it was thought that the beam settings or sampling process may not have been appropriately optimized for the analyses.

Figure 10. Dry film made from Solution #1, by drop-casting ~0.4 mL on Si wafer, and then dried overnight at room temperature. Scale bar is 100 microns (located within the red circle).

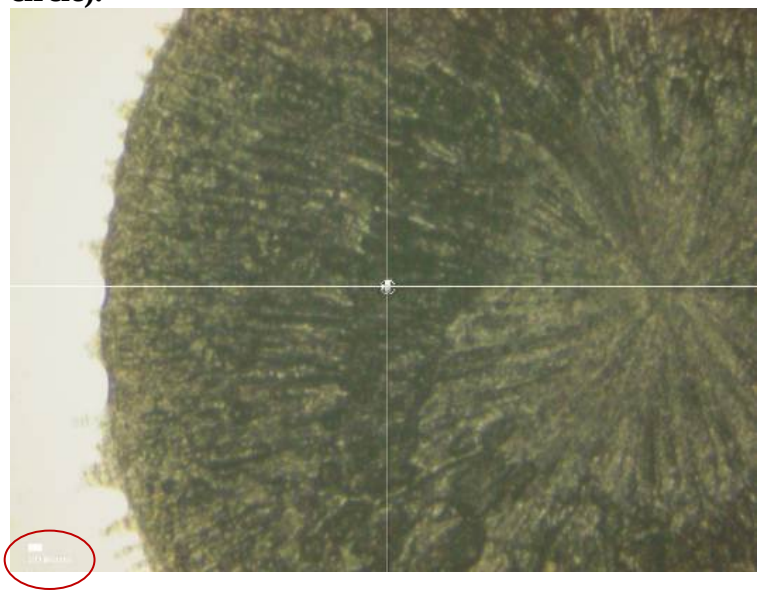

Figure 11. Solution 1 micelle film, integrated plot with d spacing values

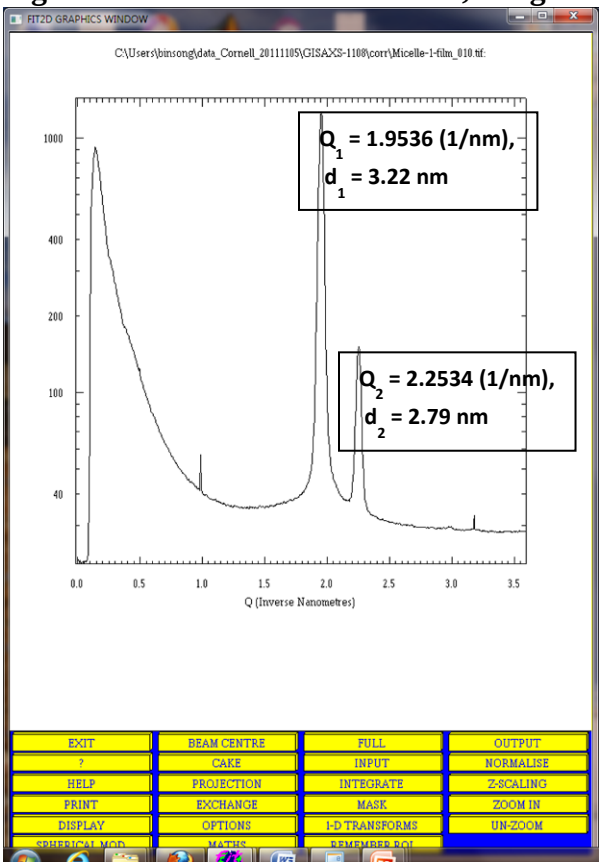

GISAXS provided evidence of particles in these solutions, although because the instrument was not optimized for these solutions, or the concentrations were too low for the instrument settings, results were inconclusive.

2.2.3. Argonne Advanced Photon Source

The purpose of the study undertaken at the Argonne Advanced Photon Source facility was to perform a controlled experiment, in which SAXS technique was used to characterize the surfactant phase changes (e.g., shape, size, etc.) of micelles following the addition of the (non-oxidizer) components within the standard DF-200 formulation - note that peroxide was not included in this study. Although the DF-200 formulation is commercially available, Sandia provided simple aqueous-surfactant mixtures representative of the surfactants within the commercial products, a sample of the commercial surfactant blend (EasyDecon Part 1) and a surfactant blend prepared in-house for comparison to the commercial surfactant blend.

The aqueous surfactant solutions provided for SAXS analyses are listed below. Note that the composition of solutions #5 and #6 are nearly the same; solution #5 was prepared in-house at Sandia National Laboratories, and solution #6 was the Part 1 surfactant mixture of the three-part commercial DF-200 product, EasyDecon.

1. Deionized water, required for background measurements
2. Cationic surfactant, Variquat 80 MC, 1.57% by weight, remainder deionized water. Variquat 80MC is comprised of 80% alkyl (60% C14, 25% C12 and 15% C16) dimethylbenzyl ammonium chloride (CAS# 68424-85-1), 20% diluent.
3. Adogen 477, 0.98% by weight, remainder deionized water. Adogen 477 (CAS# 68607-29-4) is comprised of 45-55% pentamethyltallowalkyltrimethylenediammonium dichlorides, 30-40% isopropyl alcohol, 10-20% water, and < 0.03% methylene chloride.
4. Variquat 80MC (1.57% by weight) plus Adogen 477 (0.98 % by wt), remainder deionized water
5. Solution comprised of:
    a. Variquat 80MC, 1.57 wt%
    b. Adogen 477, 0.98 wt%
    c. Propylene glycol, 9.8 wt%
    d. Potassium bicarbonate, 4.9 wt%
    e. Diethylene glycol monobutyl ether, 0.8 wt%
    f. 1-dodecanol, 0.4 wt%
    g. Isobutanol, 0.5 wt%
    h. Potassium hydroxide, 1.6 wt%
    i. Remainder deionized water, 79.45 wt%
6. EasyDecon, Part 1

This experiment was performed at the Advanced Photon Source (APS), sector 12ID-B. 12ID-B is a dedicated SAXS beam line which has simultaneous SAXS/WAXS

capability. A Pilatus 2M detector and a Pilatus 300K detector were used for SAXS and WAXS, respectively.

The set-up parameters for the experiments were: Photon energy, 12 KeV; Distance of sample to SAXS detector, 2.2 meters; Sample to WAXS detector distance, 48 cm. The SAXS analysis was performed using Igor-Pro software, with an analysis package written to fit micellar structure.

Results – (contributed by Soenke Seifert, Argonne Advanced Photon Source facility)
Background subtractions were performed using solution #1, deionized water. Solution 2, Solution 3, and Solution 4 displayed two broad peaks, but were not indicative of forming any micelle structure. The intensity of Sample 3 was observed to be lower than the Sample 2 intensity. As expected, Sample 4 (Variquat and Adogen combined) demonstrated the highest intensity. It was suggested by the analyst that particles within Samples 2, 3 and 4 could have stuck together to form hexagonal structures. This could have been the result of several months lag time between sample preparation and analysis, although samples were kept refrigerated in the interim.

Table 2. Micelle structure sizes as estimated by SAXS for solutions, #2, #3, and #4. Structures were not indicative of micelles.

Sample	1st Peak A^{-1}	Corresponding Structure Size, Angstroms	2nd Peak, A^{-1}	Corresponding Structure Size, Angstroms	Intensity, normalized
#2	0.054	116	0.116	54	1.43
#3	0.041	153	0.082	77	1
#4	0.059	107	0.119	53	2.71

Figure 12. Superimposed plots of Scattering Intensity vs. Scattering Vector, Q, for the five micelle solutions, #2, #3, #4, #5, and #6, identified above.

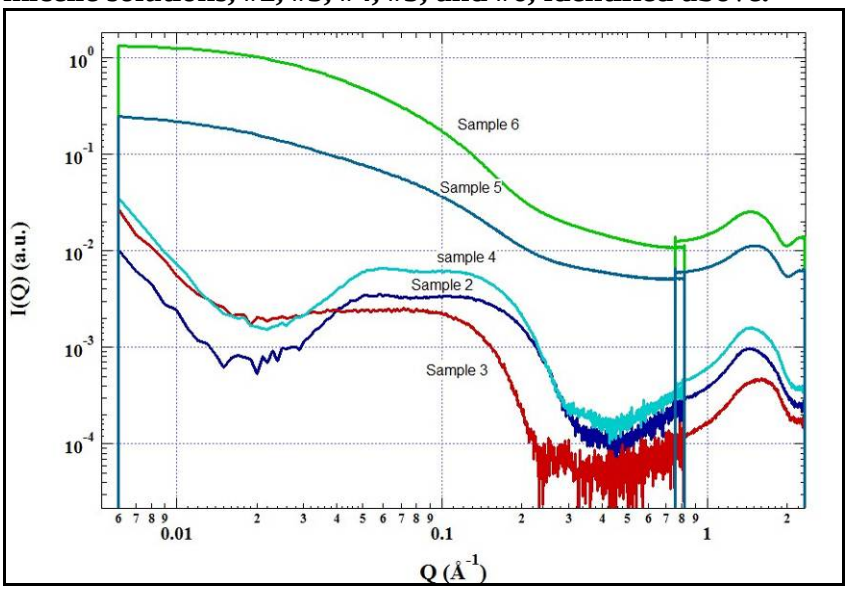

Table 3. Estimated micelle radii and diameters measured for micelle solutions #5 and #6
(SNL prepared DF-200 and EasyDecon Part 1 surfactant/co-solvent blend, respectively)

Sample	Core Radius, A	Radius of gyration	Scale Factor	Estimated micelle diameter, A	Estimated micelle diameter, nm
#5	13.7	17.3	2.25	27.4	2.7
#6	15.4	26.5	5.51	30.8	3.1

Micelle solutions #5 and #6 (SNL Part A surfactant blend, and EasyDecon Part 1) seemed to fit well to a long cylindrical core micelle structure.

The data collected at Argonne APS was gratuitously provided at no cost to the project by Soenke Seifert.

2.2.4. Conclusions of SAXS analyses

Collectively, the results obtained by the SAXS technique provided insight to the micellar structures and approximate micelle sizes of the key surfactant component within the DF-200 base formulation and a variety of prospective surfactant solutions. The SAXS analyses were performed at three different facilities using differing instrumentation and methods, without the benefit of a standardized test method. Regardless, the micelle sizes were measured to be primarily in the range of 2-3 nm. The baseline data is novel in that it served as the initial indications of the micellar environment of surfactants representative of DF-200 and other prospective CBW decontamination formulations. To be of most value, future test matrices should be expanded to collect micellar characterization data over a range of surfactant, co-solvent and ionic concentrations. Estimations of micelle particle size are presented in Table 4.

Table 4. Estimated micelle particle sizes obtained using light scattering techniques

Formulation	Data source	Mean (micelle) particle size, nm	Other
2% Berol in Lumulse	DLS (Kinnan)	Not observed	No particles could be observed for 2% Berol or 2% Variquat in Lumulse
2% Variquat in Lumulse	DLS	Not observed	
2% Variquat in DI	DLS	1	Lower concentrations of Variquat in water do not scatter enough laser light to yield reliable data.
0.1% Berol/Water	DLS	8	
0.01% Berol/water	DLS	2	
0.001% Berol/water	DLS	260	Possible interference (oil like phase) due to decrease in concentration of stabilizer in diluted Berol sample
0.61% DTAC	GISAXS (Li, Fan)	3.2, 2.7	D spacing values for dried film
0.016% LDMA	GISAXS	12.2 (real?)	D spacing values for dried film
0.61% DTAC + 0.016% LDMA	GISAXS	3.2, 2.7	D spacing values for dried film
0.61% DTAC, 0.01% LDMA, 1.65% propylene glycol, remainder DI water	GISAXS	3.0, 2.9, 2.63	D spacing values for dried film
Variquat 80MC/ Adogen 477	SAXS (Seifert)	2.7	
EasyDecon, Part 1	SAXS	3.1	

Because the SAXS capability does not exist at Sandia National Laboratories, the SAXS data was required to be collected externally, with relatively high associated expense and time required for proposal and contractual processes, as compared to the quantity of data obtained. In contrast, the PFG NMR analyses yielded significantly more useful information at much less greater expense.

2.3. Cryo-Transmission Electron Microscopy

The cryo-TEM images were collected by personnel at the UMN Characterization Facility using a FEI Tecnai G^2 F30 Field Emission Gun Cryo Transmission Electron Microscope. Samples were plunge frozen in liquid ethane using an automated plunge freezing device, known as the Vitobot. The vitrified samples were imaged at liquid nitrogen temperatures. As high magnification and resolution are critical, the magnification was appropriate to fully distinguish an individual micelle, or a small cluster of micelles. Although UMN recommended a maximum of 1 wt% of all non-aqueous components, as non-aqueous solvents present problems for plunge freezing, solutions were provided at near use concentrations ranging between 1-2%.

Cryo-TEM preliminary results indicated that the Variquat shape was spherical, ranging from 15-25 nm, and are shown in Figure 13.

Figure 13. Cryo-TEM image of 2% Variquat in deionized water

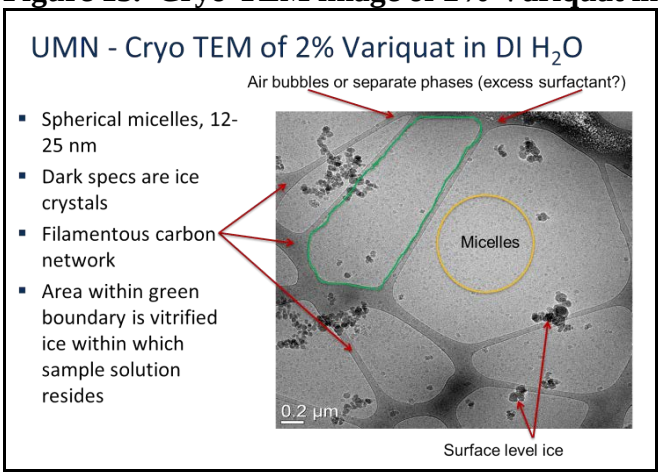

2.4. Nuclear Magnetic Resonance (NMR)

Pulsed Field Gradient Nuclear Magnetic Resonance (PFG NMR) is a technique commonly used to evaluate the characteristics of micelles in solution. Partitioning (incorporation) of various components into micelle structures, changes to micelle size and shape, and changes in the micellar phase can all be evaluated using this powerful technique. The localization of components in a solution may be used to approximate or explain solution dynamics and kinetics, final product properties and performance. Hence, it is desirable to know the component range and changing micellar aspects of prospective decontamination formulations.

Nuclear Magnetic Resonance (NMR) was utilized to generate data demonstrating baseline micellar environments in DF-200 and other micellar environments characteristic of developmental decontaminant solutions. H Pulsed Field Gradient (PFG) NMR techniques are commonly used to characterize micelles and their formation, determine partitioning coefficients, and other micelle properties (e.g., Hickok, et.al, and Gharibi, et.al.) All NMR spectra were obtained under standard PFG NMR experimental conditions on a Bruker Avance III 600 instrument operating at 600.1 MHz.

2.4.1. Micelle Formation and Diffusion (Partitioning) Study – performed by Todd Alam

A multi-phase micelle formation, partitioning and properties test study plan was developed and is described in the following sections. Developmental cationic and anionic surfactant systems were evaluated. Micelle size estimations were also provided. Results are presented for each phase of the micelle partitioning study.

2.4.1.1. Phase 1 – Baseline investigation into properties of Dodecyltrimetyl ammonium chloride (DTAC), a cationic surfactant.

The purpose of Phase 1 was to utilize PFG NMR to measure the diffusion coefficients of DTAC in water at standard temperature (298°K), as a function of surfactant concentration. This would

allow the confirmation of the Critical Micelle Concentration (CMC), published by Bahri et al., to be 20 mM or 0.539 wt%. The partitioning of the DTAC surfactant between micelle and free solution could also be determined, answering the question of whether or not this mixture follows standard mixing theory in this regime. The aging characteristics of the DTAC solution at the target concentration over a 24 to 48 hour window were monitored.

Figure 14. Structure of DTAC, dodecyl trimethyl ammonium chloride

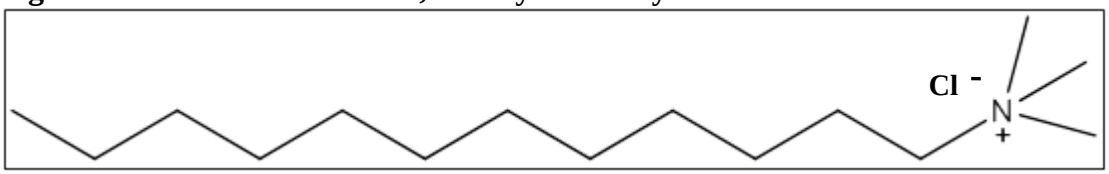

The impact to the micelle environment as formulation components are added to developmental decontaminant mixtures was a key outcome sought in this project. Through solution efficacy tests derived under another project, the addition of small quantities of N, N-1-dimethyl-1-dodecanamine was favorable to the kinetic destruction of chemical agent simulants in the solution phase. PFG NMR was utilized to investigate the diffusion properties of the DTAC/N, N-dimethyl-1-dodecanamine solution. This study was performed with a variation of total DTAC concentration and a fixed (0.0165 wt%) concentration of the amine. This study sought to provide information regarding the inclusion of this compound and impact to the micelle formation in DTAC, as well as whether or not the amine is incorporated into the micelle, remains free in solution, or some variable in between.

In a similar fashion, the inclusion of K_2CO_3 and impact to micelle formation was also determined. Ultimately, the use of PFG to compare individual component additions to a combined mixture of DTAC, NN-dimethyl-1-dodecanamine, propylene glycol and K_2CO_3 was performed.

Along the path, PFG NMR was used to look at the diffusion properties of water in each of these component solutions to determine the impact on obstruction. In the micelle structure, this effect should be minimal, and well defined, but if a vesicle structure is formed then the PFG NMR results should reflect this.

Potential technical issues that were anticipated and overcome included the requirement for unique NMR signatures for each component, adequate resolution of similar resonances among like chemical structures. The reader is directed to the referenced literature by Soderman and others for an overview of techniques this area.

Results of Phase 1

Pulse field gradient (PFG) NMR diffusion measurements of DTAC surfactant under varying conditions were collected and outlined below:

a) DTAC in D_2O 100 mM to 5 mM
b) DTAC (100 mM to 5 mM) + 0.0165 wt% dimethyl dodecamine in D_2O
c) DTAC (100 mM to 5 mM) + 1.65 wt% propylene glycol in D_2O
d) DTAC (100 mM to 5 mM) + 15.37 wt% K_2CO_3 in D_2O

In addition the 100 mM DTAC solution was monitored over several weeks for evolution of micelle structure.

1. Diffusion of DTAC at different concentrations.

Figure 15 shows the self-diffusion rate of DTAC as a function of DTAC concentration in D_2O. As expected there is a general decrease in the diffusion rate with increasing concentration between 5 and 20 mM, at which point there is a discontinuity with an increasing rate of diffusion rate reduction. This continuity occurs at the critical micelle concentration (CMC) of 20 mM, which is consistent with literature values. Before CMC the DTAC molecules are unassociated and dissolved in the solvent, above CMC a portion of the total concentration aggregate to form micelles. These micelles diffuse slower, and as such the observed diffusion constant is reduced. The effective (or measured) diffusion constant D_{eff} is given by the weighted average of the free (unaggregated) DTAC molecules diffusion rate and the diffusion rate of the micelle formed.

$$D_{eff} = c_{free} D_{free} + (1 - c_{free}) D_{micelle}$$

(Equation 1, calculation of Effective Diffusion constant, D_{eff})

Equation 1 was fit to results in Figure 15 to obtain $D_{micelle}$ which will be used in a later section to estimate the average micelle dimensions.

Figure 15 also shows the diffusion rate of water as a function of DTAC concentration. There is a gradual decrease, but there is no discontinuity at the CMC. This is also predicted for micelle systems since water is NOT expected to become associated within the micelle to any large extent. These results also show that extended range structure are not formed that interfere with the diffusion of water on the length scale of 5- 7 μm (which is the diffusion length probed by the present experimental conditions). The 100 mM DTAC solution did not show changes in the diffusion rates over several week time period, thus demonstrating equilibration. The results in Figure 15 are for freshly prepared samples.

Figure 15. The diffusion rate of D_2O as a function of DTAC concentration

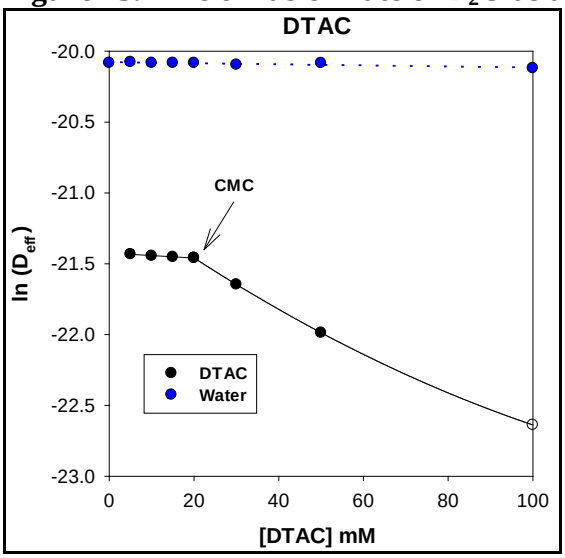

2. Diffusion of DTAC as different concentration in the presence of dimethyldodecamine.

Figure 16 shows the variation of the DTAC micelle with increasing concentration, in the presence of 0.0165 wt% lauryl dimethyl amine (dimethyldodecamine). The trends are very similar to the pure DTAC with a discontinuity observed at a CMC = 20 mM. This result shows that the addition of the amine does not change the CMC. For this mixture the diffusion rates decrease slower that in pure DTAC and reflect a decreased micelle size formation with the addition of the amine. This most likely reflects a partial charge screening afforded between the surfactant and the water solvent. The micelle size will be discussed in a later section.

Figure 16. The variation of DTAC micelle formation with increasing concentration of dimethyldodecamine

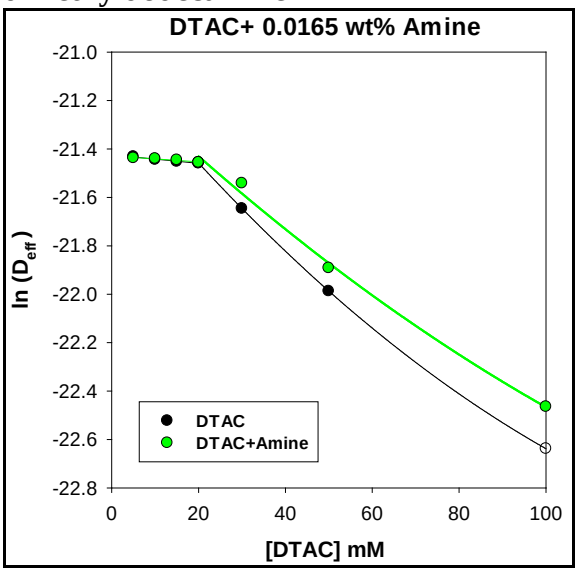

3. Variation of DTAC diffusion with concentration in the presence of 1.65 wt% propylene glycol

Figure 17 shows the variation of DTAC diffusion rates in the presence of 1.65 wt% propylene glycol. While the trend is similar to that observed for just DTAC, there are some subtle differences. Continuity is still observed at CMC of 20 mM, but at concentrations lower than this there appears to be a more rapid reduction in the diffusion rate than that was observed for pure DTAC. This effect is most likely due to partial or incomplete aggregation prior to the 20 mM CMC. This may be an equilibrium effect; however the time evolution of these solutions was not followed, but instead measured immediately after solution formation. Following the CMC, the diffusion rates are slower than in pure DTAC suggesting an increase in micelle size (see later section).

Figure 17 also shows the measured diffusion rate for propylene glycol (red triangles) as a function of DTAC concentration. The gradual decrease, without an apparent change at the DTAC CMC demonstrates that the propylene glycol is NOT incorporated into the micelle in this mixture.

Figure 17. The variation in DTAC diffusion rates in the presence of 1.65 wt% propylene glycol (green), and the measured diffusion rate for propylene glycol as a function of DTAC concentration (red triangles)

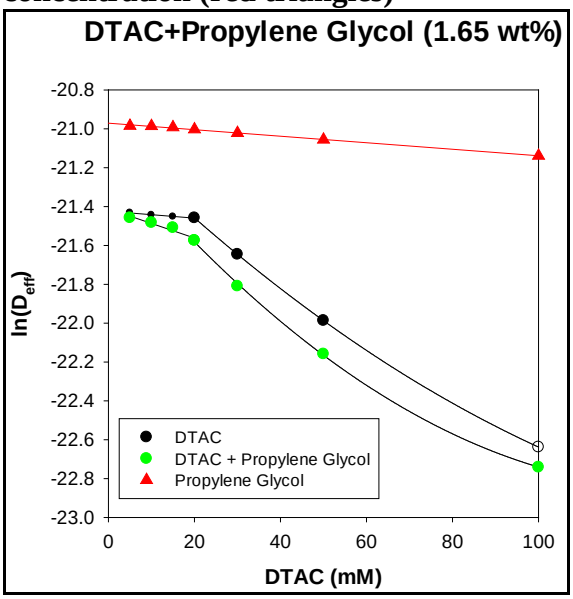

4. Variation of DTAC diffusion with variation of ion concentration in the presence of K_2CO_3.

Figure 18 shows the variation of the DTAC diffusion rates in the presence of carbonate. The behavior is markedly different. First there does not appear to be a CMC near 20 mM. The CMC is now < 2 mM in the presence of the carbonate and above 20 mM there is a final formation of equilibrate micelle sizes. An extended structure does not appear to be occurring as the water diffusion rates are close to that observed for the pure DTAC solution. This system also showed evolution over several hours at high DTAC concentration, bringing a kinetic aspect to these

results. These results are not fully understood and some additional experiments with decreasing carbonate concentration are recommended.

Figure 18. Variation of DTAC diffusion rates in the presence of potassium carbonate

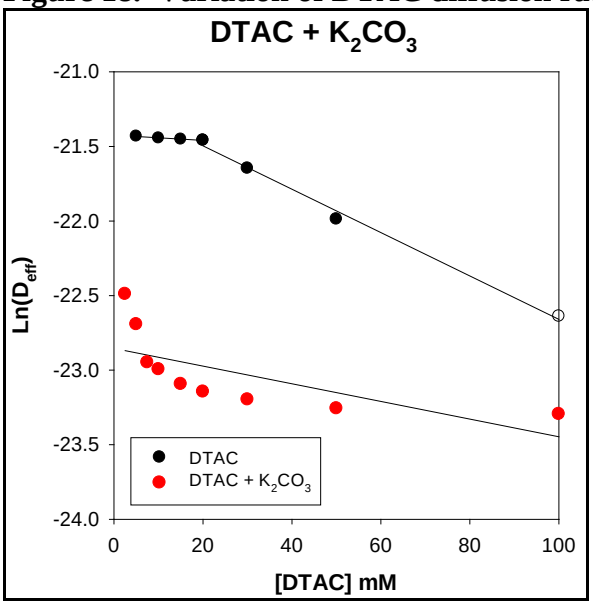

5. Estimation of micelle size for different solutions.

By fitting Equation 1 to the results in Figures 15 -18 the diffusion rate of the micelles can be determined. From this the effective hydrodynamic radius of the micelle is estimated using the Stokes-Einstein equation:

$$R_H = \frac{k_b T}{6\pi\eta D_{micelle}}$$

where the viscosity of D_2O at 298 K was used as an estimation. The contour length of DTAC is 18.4Å such that these estimated micelle radius were consistent. As determined from the qualitative description of the diffusion behavior, the addition of the amine results in a smaller micelle, while the addition of propylene glycol to the mixture increases the micelle size (but does not become directly incorporated into the micelle).

Table 5. Estimated effective micelle radius at 100 mM DTAC concentration

Sample	**R_H(Å)**
DTAC	24.4
DTAC + amine	17.1
DTAC+ propylene glycol	31.4
DTAC + K_2CO_3	N/A

2.4.1.2. Phase 2 - Analogous investigations using the anionic surfactant, sodium lauryl sulfate. The purpose of Phase 2 was to perform pulse field gradient (PFG) NMR diffusion measurements of SLS surfactant under varying conditions. These included:

a) DTAC in D_2O 100 mM to 5 mM
b) DTAC (100 mM to 5 mM) + 1.65 wt% propylene glycol in D_2O
c) DTAC (100 mM to 5 mM) + 10, 5 and 2.5 wt% wt% K_2CO_3 in D_2O

Experimental:
All NMR spectra were obtained under standard PFG NMR experimental conditions on a Bruker Avance III 600 instrument operating at 600.1 MHz.

Results of Phase 2:

1. Diffusion of SLS at different concentrations.

Figure 19 shows the self-diffusion rate of SLS as a function of SLS concentration in D_2O. As expected there is a general decrease in the diffusion rate with increasing concentration between 2.5 and 8 mM, at which point there is a discontinuity with an increasing rate of diffusion rate reduction. This continuity occurs at the critical micelle concentration (CMC) of ~8 mM, which is consistent with literature values (8.2 mM at 25 ^oC). Before CMC the SLS molecules are unassociated and dissolved in the solvent, above CMC a portion of the total concentration aggregate to form micelles. These micelles diffuse slower, and as such the observed diffusion constant is reduced. The effective (or measured) diffusion constant D_{eff} is given by the weighted average of the free (unaggregate) DTAC molecules diffusion rate and the diffusion rate of the micelle formed.

$$D_{eff} = c_{free} D_{free} + (1 - c_{free}) D_{micelle} \quad (1)$$

Equation 1 was fit to results in Figure 19 to obtain $D_{micelle}$ which will be used in a later section to estimate the average micelle dimensions.

Figure 19. Self-Diffusion of Sodium Lauryl Sulfate (SLS)

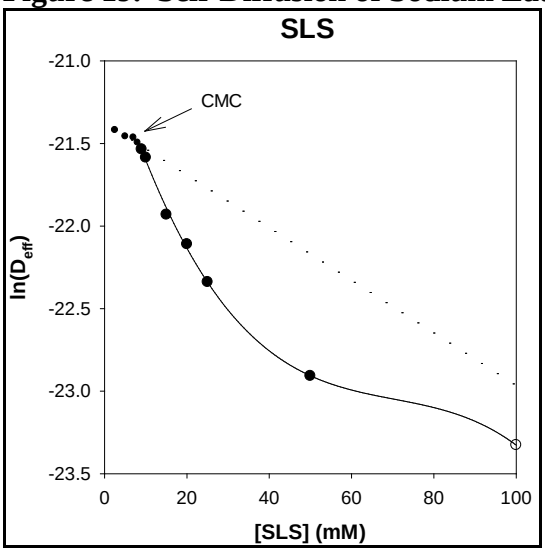

2. Estimation of micelle size for SLS solutions.

By fitting Equation 1 to the results in Figure 19 the diffusion rate of the micelle can be determined. From this the effective hydrodynamic radius of the micelle is estimated using the Stokes-Einstein equation

$$R_H = \frac{k_b T}{6\pi\eta D_{micelle}}$$

where the viscosity of D_2O at 298 K is used for estimation. SLS has a fully extended contour length of ~ 18 Å.

Table 6. Estimated effective micelle radius at SLS solutions above the CMC.

Sample	**R_H(Å)**
100 mM	50.7
50 mM	45.4
25 mM	28.4
20 mM	19.5
15 mM	19.6

3. Diffusion of SLS with K_2CO_3.

SLS solutions (100 mM) containing 2.5, 5 and 10 wt% K2CO3 precipitated out of solution due to the formation of large, extended structures. This precluded the measurement of diffusion rates, or the calculation of a micelle radius for these solutions.

4. Variation of SLS diffusion with concentration in the presence of 1.65 wt% propylene glycol

Figure 20 shows the variation of SLS diffusion rates in the presence of 1.65 wt% propylene glycol. This behavior is almost the same as observed for DTAC + Propylene glycol. Following the CMC the diffusion rates are slower than in pure SLS reflecting an increase in the micelle size. Figure 20 also shows the measured diffusion rate for polypropylene glycol (red triangles) as a function of SLS concentration. The gradual decrease, without an apparent change at the SLS CMC demonstrates that the propylene glycol is NOT incorporated into the micelle in this mixture.

Table 7. Estimated effective micelle radius at SLS + propylene glycol solutions.

Sample	**R_H(Å)**
100 mM	71.8
50 mM	104.9

Figure 20. Variation of SLS diffusion rates in the presence of propylene glycol

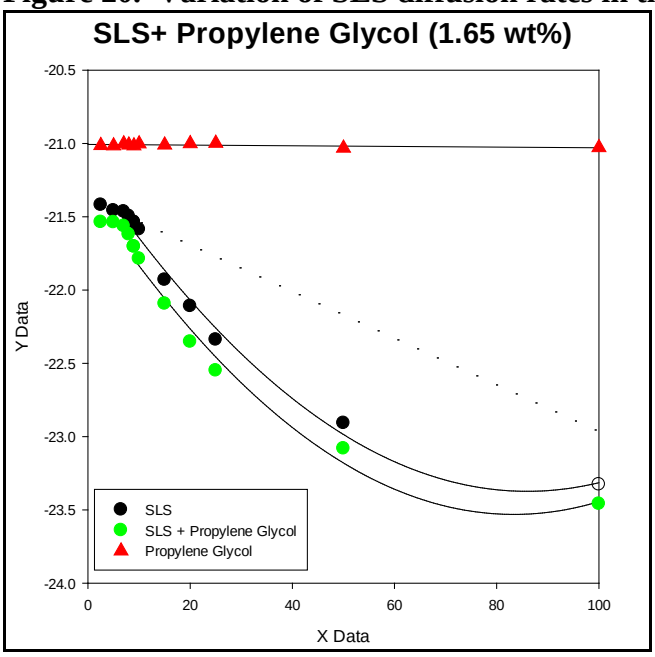

2.4.2. NMR – Summary of micelle partitioning tasks

Through this task, diffusion properties of key surfactants were measured and their impact to surfactant micelle size and shape upon addition of components was determined. The surfactant partitioning from micelle formation vs. free in solution was monitored. Significant impacts to CMC, micelle diffusion rates and micelle size, in some cases were observed. The diffusion properties of surfactants in various solution mixtures were measured, to infer potential phase changes.

In total, the results of the NMR micelle diffusion and partitioning tasks not only provide fundamental physiochemical properties of various surfactant solutions, but aid in the deduction of desirable micelle properties and components. The process of deducing desirable properties remains ongoing, as we are currently contrasting decontamination efficacy of agents in solution and on contaminated surfaces to physiochemical and diffusion properties of various prospective decontamination formulations.

2.5. Micellar Characterization Conclusions

Micellar characterization of limited surfactant solutions was performed externally through the collection and measurement of Small Angle X-Ray Scattering (SAXS) images and Cryo-Transmission Electron Microscopy (cryo-TEM) images. Micellar characterization was performed externally at the University of Minnesota's Characterization Facility Center, and at the Argonne National Laboratory Advanced Photon Source facility. Several surfactant-based decontamination solutions were evaluated, including the commercially available DF-200 Part 1 surfactant blend. Across all solutions tested (both cationic quaternary ammonium compound-

based, and the anionic surfactant, sodium lauryl sulfate), results indicated an average micelle size of approximately 3 nm.

A micellar diffusion study was conducted internally at Sandia to measure diffusion constants of surfactants over a concentration range, to estimate the effective micelle diameter, to determine the impact of individual components to the micellar environment in solution, and the impact of combined components to surfactant phase behavior.

The data and observations collected throughout the task substantiate the concept of micellar catalysis in general. The cationic surfactant species appear to be necessary for highly reactive formulations suitable for the decontamination of CWAs or toxic chemicals that are water insoluble, or slightly water soluble. With respect to the SLS anionic surfactant, it can be concluded that anionic surfactant micelles do not provide favorable kinetic conditions for either water insoluble or water soluble toxic chemicals (as compared to the kinetics observed by cationic DTAC reactive solutions and supported by SLS-specific data obtained under a separate WFO project). The breakdown of water soluble chemicals may be favored in the free, bulk solution state, and not within the micelle.

3. DF-200 AEROSOL DROPLET CHARACTERIZATION

3.1. Introduction

One of the primary goals associated with this LDRD project is to determine how the DF-200 formula behaves in aerosolized droplet form. Among the behaviors of interest are overall particle evaporation rates and the DF-200 surfactant concentration in the droplet over time when exposed to ambient conditions and varying parameters on the rotary atomizer by Illinois Tool Works (ITW Nozzle). Particular focus for the data presented here is given to the voltage applied to the nozzle during spray dispersion and the effect of relative humidity on droplet evaporation characteristics.

A solution droplet will either take on water or evaporate according to both the curvature (size) of the droplet and the amount and type of solute contained in solution with water. The curvature works to increase the saturation vapor pressure required for the droplet to begin taking on water and thereby increasing the evaporation rate when exposed to relative humidity below activation. The quantitative representation of this process is given by the Kelvin equation. For saturation vapor pressure dependent on pressure and temperature over a flat liquid water surface the following exponential relation applies:

$$e_s(T,p) = e_s(T) exp\left[\frac{p}{R_v T \rho_w}\right]$$

where R_v is the gas constant, p is the atmospheric pressure, e_s is the saturation vapor pressure, and ρ_w is the density of water. This equation can be expanded to include the effect of curvature of a liquid droplet on condensation and evaporative processes by investigating the saturation vapor pressure at the droplet surface.

$$e_s\,(T,p_d) = \; e_s(T,p)\,\exp\left[\frac{2\sigma}{R_v T \rho_w a}\right]$$

where p_d is the pressure of the liquid on the droplet surface, σ is the surface tension of water, and a is the droplet radius. This can be further approximated through Taylor series expansion to reduce the atmospheric pressure dependence and simply for calculation purposes to:

$$e_s\,(T,p_d) \approx \; e_s(T)\left[1 + \frac{a_k}{a}\right]$$

with,

$$a_k = \frac{2\sigma}{R_v T \rho_w}$$

The effect of a solute added to the droplet works to decrease the saturation vapor pressure required for a droplet to begin taking up water. This is detailed through Raoult's Law considering the activity of the solution droplet such that

$$X = 1 - \frac{n_s}{n_w}$$

in its simplest form considering a single component solution droplet. n_s is the number of moles of solute, and $n_w$is the number of moles of water in solution. It follows then that,

$$X = 1 - \frac{3 m_v M_s}{4\pi m_s \rho_w a^3} \equiv \left(1 + \frac{a_s}{a^3}\right)$$

Combining the definition of saturation vapor pressure for a pure water droplet due to curvature and for a solute, we arrive at the following deterministic equation:

$$\frac{e_s(T,p_d,X)}{e_s(T)} \approx \left(1+\frac{a_k}{a}-\frac{a_s}{a^3}\right)$$

which is the Taylor Series expansion of the solution. By definition, $\frac{e_s(T,p_d,X)}{e_s(T)}$ is the supersaturation relative humidity for the solution droplet. As depicted in Seinfeld and Pandis, 1998, the solution to this equation is shown in Figure 21. The activation humidity depicted in Figure 21 can be obtained mathematically from the equation above for a given single component solution droplet. Since our experimental conditions require the dispersion of a solution droplet containing multiple solutes, we will use the previous equations as a guide to describe how these droplets should and do behave in the environment.

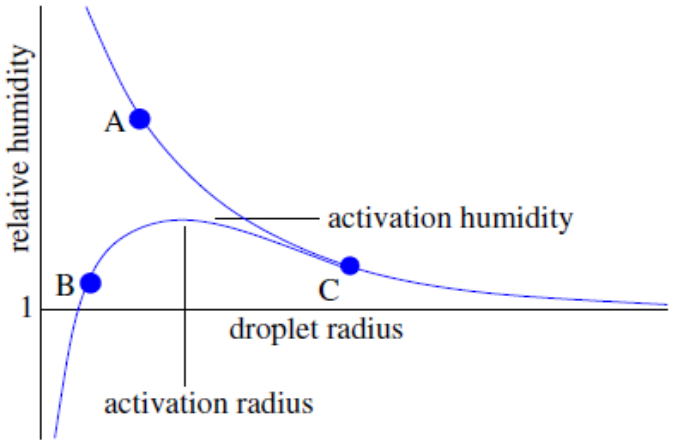

Figure 21. From Seinfeld and Pandis, 1998: solution to the equation for the supersaturation of a solution droplet. The relative humidity of 1 refers to 100% RH.

The most notable characteristic of a DF-200 droplet population dispersed using the ITW nozzle is that these droplets are at their activation humidity upon generation because they are generated as a liquid aerosol. Therefore, based on Figure 21 above, this droplet will then evaporate falling down the left side of the activation curve toward point B. If the relative humidity remained above 100% as it does in a cloud, the droplets would continue to grow while the required growth supersaturation continued to decrease as the droplet size increased.

This process of activation followed by growth and consequently evaporation has been extensively studied using a humidified tandem measurement system as is shown in Figure 22 from the studies of Kulmala et al, 2001 and Joutsensaari et al, 2001. For this study, a pure sodium chloride salt particle was exposed to increasing relative humidity values until it begins to take on water at around 78% relative humidity. The growth factor in the figure below is defined as the ratio of the wet (activated) diameter to the dry (crystalline) diameter. Therefore, the growth factor is a direct measure of the amount of liquid water contained in the particle. The point at which a particle activates and takes on water is the deliquescence point. Following activation, the droplet will continue to grow. Consequently, the point along the hysteresis (wet evaporation curve – open circles) where the particles suddenly crystallize (crystallization point) is not equal to the deliquescence point as indicated in Figure 22. Since the DF-200 droplets are

being generated in activated form (>95% RH), we will see that these droplets follow an exponential decay hysteresis in agreement with theory although not identical to a pure NaCl salt solution droplet. The scope of this work did not allow for the determination of droplet activation diameter or crystallization point.

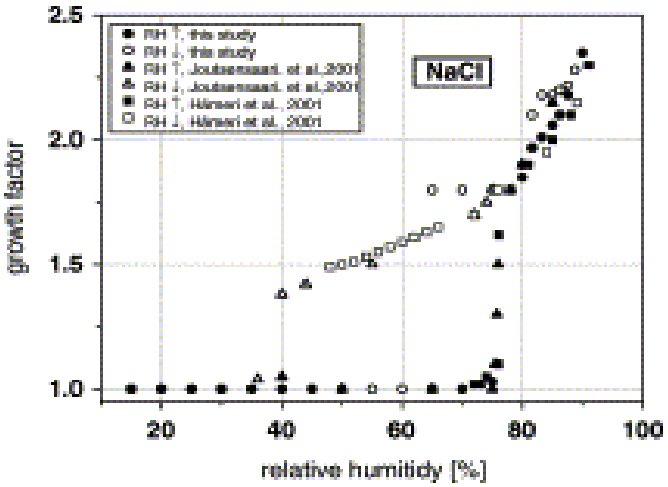

Figure 22. Deliquescence and Hysteresis for pure NaCl salt particles.

3.2. Methodology

3.2.1. Aerosol Characterization Experimental Setup – ITW Rotary Atomization Nozzle

Commercially available DF-200 decontamination formula was aerosolized using a rotary atomizer system manufactured by Illinois Tool Works (ITW) Finishing Group. This technology, originally developed for uniform paint spray applications, breaks up liquid into a broad range of micron-sized droplets. Previously used for assessing the dispersal of electrically charged droplets, the ITW nozzle, shown in Figure 23, generates a reproducible aerosol size distribution given a specific set of test parameters. The ITW Nozzle's mechanical operation details are outlined in the Aerosolized Activated Hydrogen Peroxide (AAHP): Final Report (SAND 2009-5761). For the purposes of this study, the ITW nozzle mechanical parameters were set to the following using a specially designed 45-mm aluminum cup: an applied voltage equal to either 0 or 3 kV, a shaping air flow rate of 100 SLPM, and a cup velocity of 30,000 RPM. The cup velocity was chosen to provide a broad aerosol size distribution containing a larger fraction of particulates in the 1 µm to 3 µm range bins.

Prior to each experiment, the ITW nozzle was purged of residue using first deionized water and then air to ensure that all lines were cleaned of any pre-existing materials. Following line purging, the ITW reservoir was filled with Sandia's non-modified DF-200 formula, and a liquid flow rate was determined by sampling a volume of material for a set period of time; weight was determined prior to and after liquid volume sampling. The target achievable liquid flow rate was near 10 lpm.

Figure 23. Photo of ITW Rotary Atomizer Nozzle and Mechanical Control Unit

3.2.2. Aerosol Characterization Particle Test Chamber Experimental Setup

Upon the successful setup of the ITW nozzle, a spray volume of aerosolized DF-200 was injected into a 281 L static-free acrylic chamber and continuously mixed using an internally mounted 5-inch CPU fan as depicted in Figure 24. The mixing chamber was wrapped with 3/8 inch copper tubing as shown in Figure 25, which was used to circulate either cooled or heated 50/50 mix of propylene glycol and water allowing for temperature control within the small volume chamber. Temperature and Relative Humidity were measured using a Omega RH probe and data recorded using the manufacturer provided data-logging software.. The suspended aerosol within the chamber was intermittently sampled using a TSI Corporation Aerodynamic Particle Spectrometer (APS). The APS works on the principle of single aerosol particle transport. Each particle that passes through the measurement volume is counted and sized using a 680-nm diode laser source. Sampling intervals were determined experimentally to provide the least amount of particle loss due to sampling while maintaining the integrity of the measured volume. The aerosol population was sampled for a two-minute period (2.33 min) every 15-min for the duration of the experiment (2.33 min of chamber sample followed by 12.67 min of filtered ambient air) using a LabView data acquisition automated program. In an effort to further limit the mass of aerosol lost to sampling times and facilitate an increased measurement period, a 5 to 1 dilution flow was used in line with the APS. Data was collected and logged using the standard TSI Automated Instrument Management System (AIMS), a data acquisition program provided by TSI for instrument control and data communications.

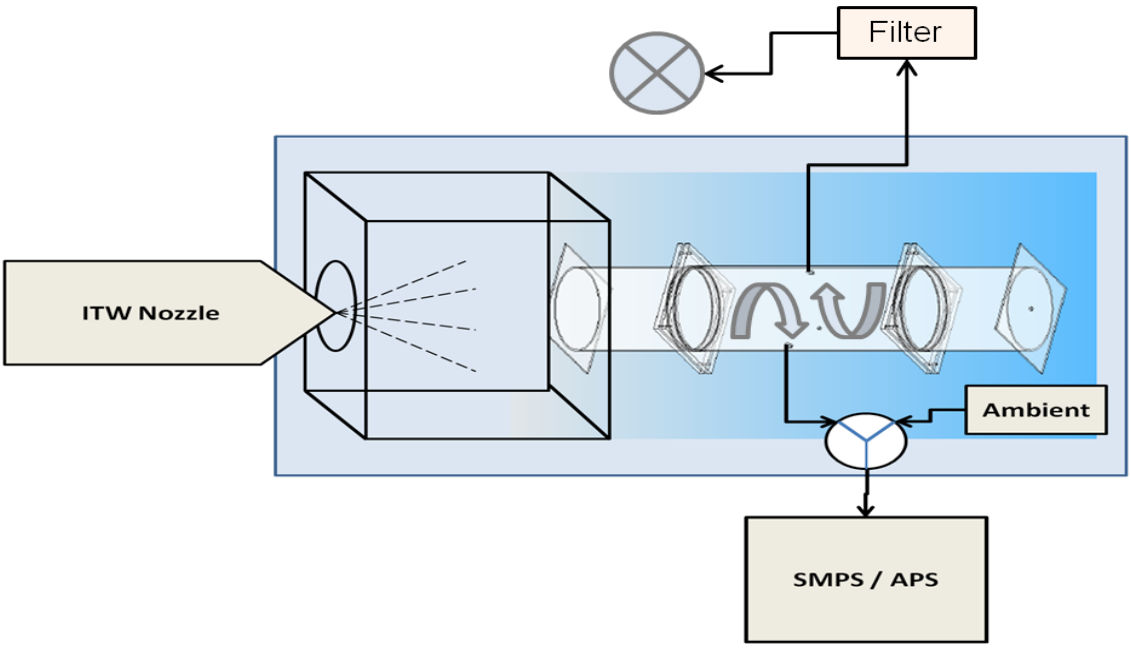

Figure 24. Schematic of the aerosol mixing chamber, nozzle injection position, and sampling mechanisms

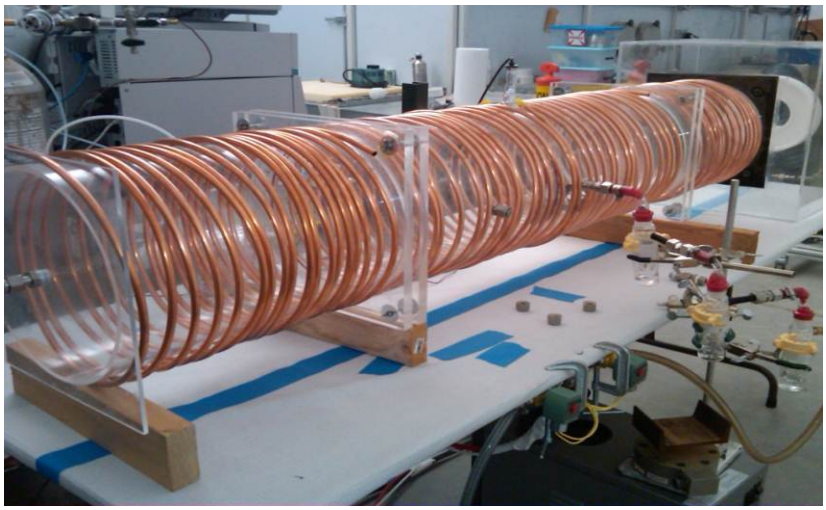

Figure 25. Photo of the chamber with coiled temperature control

3.2.3. Aerosol Characterization Test Procedure

Filter samples of the suspended aerosol particles were also collected during the 2.33 sampling period of the APS in order to provide a representative mass measurement as well as extract chemical information using a GC/MS system. Each 25-mm filter, manufactured by Pall Corporation, Life Sciences Division, were type A/C glass fiber filters (#61630, lot 725431), was housed in a stainless steel filter canister and connected to the mixing chamber. The filter holder was connected to an external pump where the flow rate was controlled using a 4.91 lpm critical orifice. Prior to the filter insertion within the stainless steel container, pre-experimental filter weights were obtained using a 5-digit laboratory grade weigh balance.

Because of the balance sensitivity and the process of DF-200 chemical constituent extraction (detailed in section 3.2.4), filter-pre-weights were determined along with a standard laboratory grade weigh boat. First, the balance was allowed to settle and then tared. Second, a weigh boat was placed inside the glass sealed scale housing, and the scale was again tared. A single 25-mm glass fiber filter was then weighed in the weigh boat and the weight recorded as the filter pre-weight. Lastly, both the filter and the boat were placed in a Ziploc bag and labeled accordingly. Following sample collection, the filters were immediately removed from the filter housing and returned to the properly labeled Ziploc bag face down in the weigh boat for post-test weight determination. The filter/boat combination is then placed in the corresponding glass jar, 7 ml of iso-octane added, and the entire unit is placed on an orbital shaker for no less than 30 min. This method ensures that the majority of the DF-200 solution droplets collected on the filter is dissolved into the iso-octane liquid to allow for GC/MS analysis methods.

At the beginning of the testing, a TSI Scanning Mobility Particle Sizer (SMPS) was connected in an effort to measure the drop size distribution less than 0.5µm. However, little to no evidence exists which suggests that these liquid droplets were being detected by the system. This is likely due to a combination of unfavorable collection parameters including significant particle losses of the water droplets within the internal sampling system of the SMPS and water Condensation Particle Counter (CPC).

Initial testing required that the spray volume in the chamber reach an integrated aerosol concentration near 10^4 particles/cm^3. By limiting the injection time in this manner, the relative humidity remains below 65% for the duration of the experiment. Based on the hysteresis for a salt-solution aerosol, a relative humidity below this limit will place the droplets in an environment well below activation and thereby remove the possibility that droplet growth will impact the population dynamic. The results from these tests also enabled the experimental determination of particle residence times within the chamber which led to the final experimental setup and test design detailed above. This test condition was applied with both 0 kV and 3 kV charge dispersion to provide for comparative analysis of the physical properties between a charged and uncharged droplet population. Monitoring the droplet size distribution over time under approximate environmental and specific generation conditions allows for the determination of the aerosol population dynamics over a one to two hour period.

3.2.4 Aerosol Characterization Analytical Methods – GC/MS Calibration and Measurement

For all methods, the MS source was set at 230° C and the MS Quad was set at 150° C. The column used was a HP5-MS, 30 meter length and 0.25mm internal diameter. The film thickness was 0.25 micron. The GC/MS was set to selective ion monitoring (SIM) mode for increased sensitivity and ease of quantitation. The compounds were identified by retention times and the three ions. The underlined ion in Table 7 below is the quantitation ion; the other two were used as qualifying ions.

Table 8. GC/MS Method Parameters

Method Name	Starting Oven Temp (C°)	Oven Ramp C°/min	Oven Hold Time (Minutes)	Injection Volume (µL)	Inlet Mode	Ion Masses (SIM)
Oleic Low	58	35 to 220°	0	2	pulsed splitless	55.1, 69.1, 264.3
		15 to 275°	0.25			
Oleic High	58	35 to 220°	0	2	split 25:1	55.1, 69.1, 264.3
		15 to 275°	0.25			
DEGMBE Low	60	20 to 220°	0	1	pulsed splitless	45.1, 57.1, 75.1
DEGMBE High	60	20 to 220°	0	1	split 25:1	45.1, 57.1, 75.1
1-Dodecanol Low	60	20 to 220°	0	1	pulsed splitless	69.1, 83.1, 97.1
1-Dodecanol High	60	20 to 220°	0	1	split 25:1	69.1, 83.1, 97.1

Calibration for all three compounds was done by serial dilutions by weight in hexane. For oleic acid, the dilutions were from 1000mg/L to 10 mg/L and for the other two compounds the range was 250 mg/L to 0.01 mg/L.

For the DF-200 components, DEGMBE and 1-Dodecanol, calibrations were done with the above listed settings for four months. The mean R^2 values, with standard deviations and % CV are outlined below.

Method	Mean R^2	Std Dev	% CV
DEGMBE Low	0.997	0.001	0.15
DEGMBE High	0.998	0.001	0.110
Dodecanol, Low	0.998	0.002	0.226
Dodecanol, High	0.999	0.001	0.051

The lower limit of detection for the DF-200 components is 0.01 mg/L on the low calibration curve and the high curves had an upper limit of around 250 mg/L. That upper limit may have been able to be raised, but was not needed for the testing requirements. Oleic acid had a lower limit of 15 mg/L and an upper limit of 900 mg/L.

3.2.5. SKC BioSamplers – Chemical Aerosol Sampling Collection Efficiency

Earlier in the project, testing was completed to evaluate the efficiency at which the SKC BioSampler impingers to collect aerosolized chemicals. The collection efficiency of the SKC BioSamplers for aerosolized chemicals was approximated by calculation in earlier works. However, the aerosol sampling collection efficiencies for the SKC BioSampler method had not been experimentally confirmed previously.

Using aerosol generation techniques described in Section 3.2.1, the test chamber was filled with aerosolized oleic acid, and aerosol sampling performed using the SKC BioSamplers with hexane as the collection solvent. Briefly, oleic acid was aerosolized to reach a concentration density of 10^3 mg/m^3 as determined by APS. The SKC BioSampler valves were initiated and aerosol samples collected for 2 minutes, using a verified SKC flow rate of 12.2 L/min. Initial testing included a series of three BioSamplers; however, a pressure differential was observed at each unit resulting in minimal flow into the second and third BioSamplers. Sufficient flow, required to adequately maintain efficient sonic "swirling" of the collection solvent, was not achieved and thus the tri-series configuration was deemed unacceptable.

Table 9. ITW nozzle parameters used for the dispersal of oleic acid during SKC BioSampler sampling efficiency analyses

ITW nozzle parameters		
ITW Spray Flow Rate (liquid):	10	**mL/min**
ITW Fluid Pressure:	13	**psi**
ITW Flow Pressure (air):	20	**psi**
Turbine Speed:	30000	**RPM**
ITW Shaping Air:	100	

Chemical aerosol sampling collection efficiency evaluations proceeded by the testing of a single SKC BioSampler. Results indicated that the SKC sampling efficiency as compared to the APS was approximately 40%, or within an order of magnitude. This value is considered acceptable, as prior works to measure the reduction of aerosolized chemical (simulant) concentrations have demonstrated several orders of magnitude reduction from initial, customer provided threat scenario concentrations down to detection levels over the 1-2 hour duration of a typical test.

3.3. Results

3.3.1. Aerosol Size Distribution Analysis

The data collected was first minimized by matching the total experimental time with that recorded in the experimental notes. A density of 0.978 g/cm^3 (the density of water at standard temperature and pressure in Albuquerque, NM) was used to process the aerosol concentration data into mass concentration for volumetric analysis of the particle population. To obtain the overall evaporation characteristics of suspended particles within the measurement chamber, the size resolved number and mass concentration retrieved from APS measurements were quantitatively reduced to include only those particles which remain suspended for the duration of a measurement cycle. A measurement cycle is defined here to be the full 15 min sampling sequence (2.33 min of sampling from the chamber followed by 12.67 min of filtered air sampling). To do this, the data was first binned according to particle size, and particles less than 0.543 µm were subtracted from the suspended aerosol concentration and allowed to be summed into the total mass within the chamber volume (here, assumed to be lost to the wall for simplicity). Particles less than 0.543 µm are sized into only one bin according to the APS sizing mechanisms. Therefore any concentration obtained for those particles remained un-resolved according to size and therefore not useful for physical analysis of the droplet population.

Second, the droplet size distribution was corrected for sampling losses in the tubing from the chamber to the APS. Particle transport efficiencies were calculated based on the diagram for tubing length and size in Figure 26 below. The resulting particle transport efficiency for a range of particles under these experimental conditions is depicted in Figure 27.

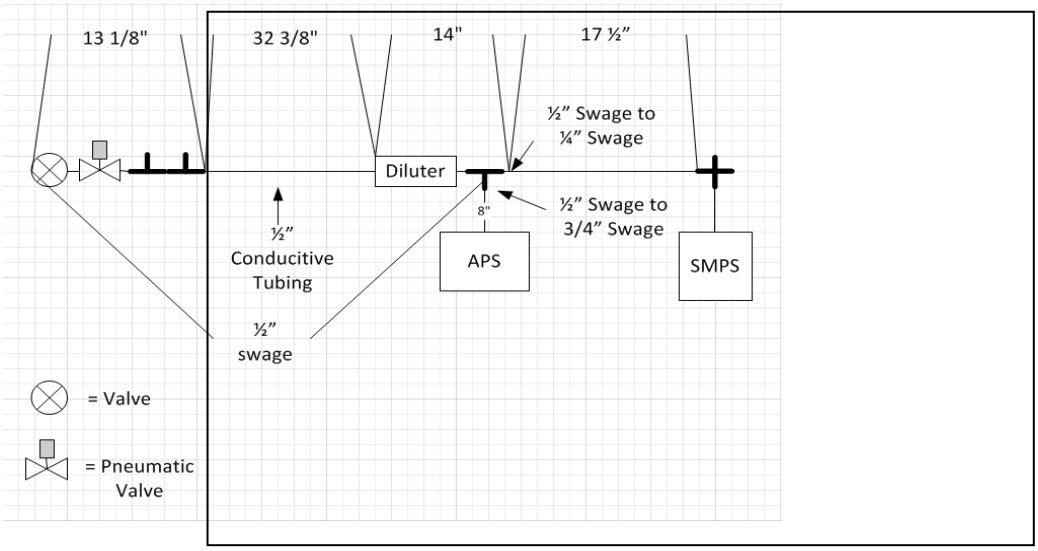

Figure 26. Schematic of aerosol sampling setup used to calculate particle transport losses

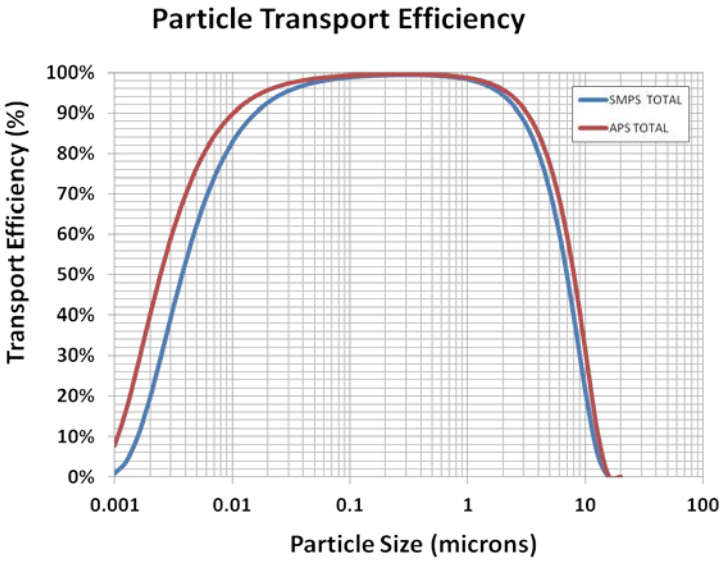

Figure 27. Results of particle transport calculations

Following the correction for losses, an iterative algorithm was used to predict the size-resolved particle concentrations that remain suspended between measurement cycles and therefore contribute to the time-resolved distribution. The particles which are determined to not remain suspended in the mixing chamber environment are assumed to be lost to the wall with minimal losses due to sampling. This was done using empirical results for the depositional velocity for particles as a function of particle size, according to the work of Slinn, et al., 1978 as presented in Seinfeld and Pandis, 1998 as a model for dry deposition calculations for a velocity of 11 cm/s. These results incorporate both gravitational settling and loss due to mixing of a particle population in a wind tunnel environment, an environment similar to the one used here.

Using this empirical calculation, particles greater than 2.0 µm are quickly and permanently lost through dry deposition processes to the walls of the chamber where they are assumed to stick with re-suspension effects not likely. This is a valid assumption, since the suspended particles are in liquid droplet form and will have no bounce effects from the wall. The calculation is performed for each measurement cycle of 2 min 20 sec. Along with particle wall loss, the concentration of particles lost due to sampling is also calculated and subtracted from the suspended distribution in a predictive manner. After removing these particles from the suspended distribution, the remaining particle distribution is used to calculate the suspended mass concentration within the chamber and, subsequently, the mean aerodynamic diameter throughout the measurement cycle. It is important to note that although a large amount of liquid droplets are being lost to the wall, these droplets will still contribute to any evaporation that occurs within the chamber and thereby the vapor phase concentration.

Mean droplet size and statistics is then determined by fitting the aerosol size distribution with log-normal curves of the form:

$$P_L\ (n\ (D_p)) \;=\; \frac{1}{(2\pi)^{1/2} n\ (D_p) \ln \overline{D_p}} \quad \exp \left[\frac{\left(\ln n\ (D_p) - \ln \overline{D_p} \right)^2}{2 \ln^2 \sigma_g} \right]$$

where $\overline{D_p}$ is the geometric mean diameter, σ_g is the standard deviation of the size distribution, and $n(D_p) = \frac{dN}{d \log D_p}$. For the purposes of this project, only the primary mode of the particle population was fit using this method in order to track the overall mean particle size over time and to eliminate false tracking of the larger particles which will eventually deposit out of the distribution.

3.3.2. Aerosol Characterization Results – Aerosol Size Distribution

Particle loss rates were monitored throughout the experiment as a verification that particle mass was conserved during data processing and to account for the total mass of DF-200 droplets in the mixing chamber. While little particle loss due to sampling was observed, a significant fraction of the initially injected size distribution is lost to the walls of the small volume mixing chamber from one sample to the next. Figure 28 shows a representative result from the data processing of mass loss. Through the remainder of the experiment, mass is lost due to the combination of sampling and deposition. Once the concentration of particles that remain suspended in the chamber reaches near 10^2 particles/cm^3, the suspended particle concentration has decreased by 100 times.

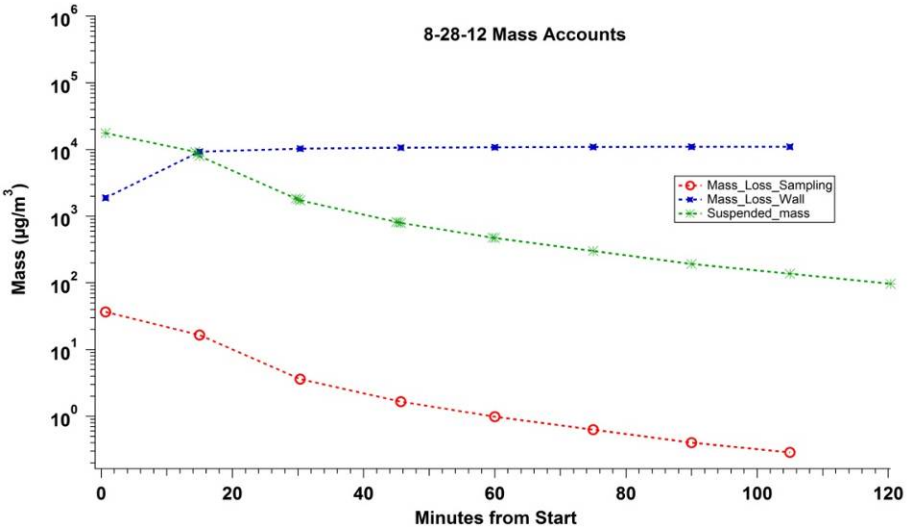

Figure 28. Representative calculations of suspended mass (green) due to wall deposition (blue) and sampling losses (red)

As with any solution droplet dispersed in liquid form containing a large fraction of water, evaporation is expected to occur along the hysteresis leg of a deliquescence curve relative to that solution droplet. Here, we were not experimentally set to determine the deliquescence of a DF-200 solution droplet. Instead, we were aiming to understand the physical behavior of a DF-200 solution droplet under differing environmental conditions.

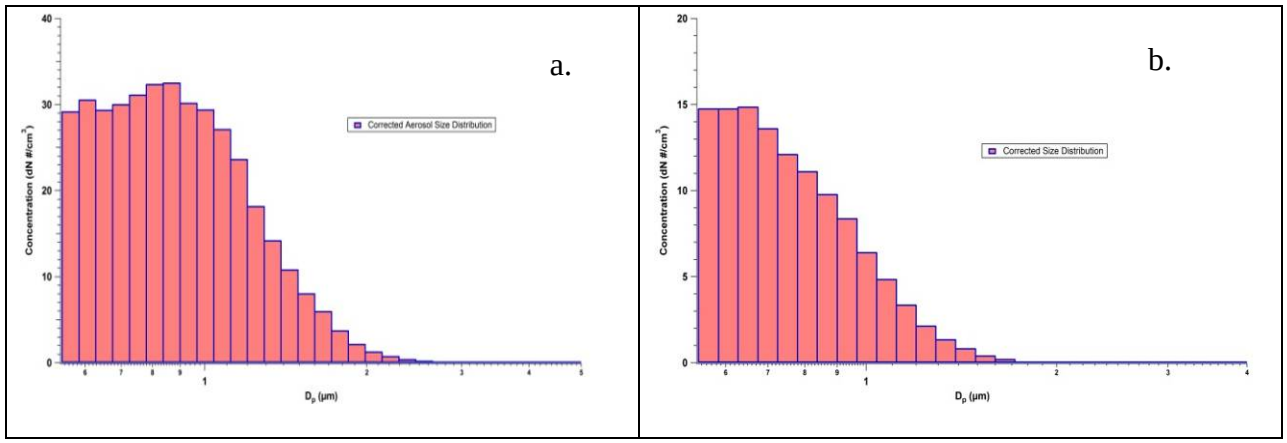

Figure 29. Representative beginning and ending size distribution for aerosol population

Figure 29 shows a representative processed aerosol size distribution at time t=0 (Figure 29a.) and at time t= 100 min (Figure 29 b.). Upon dispersion of DF-200 droplets into the mixing chamber, the peak of the size distribution is generally around 1.0 µm once the larger particles that settle out quickly have been removed from the droplet population using the iterative process described in section x. Following 100 minutes of residence time in the mixing chamber, the size distribution has shifted to smaller sized particles in agreement with the theory of droplet evaporation described in Section 3.1. As indicated the peak diameter for the final suspended distribution is between 0.50 and 0.70 µm. This result, as will be shown in subsequent sections, remains constant regardless of the environmental or initial droplet spray conditions. However, the rate of decrease in particle size will vary based on conditional experimental controls. Figure 30 gives the standard deviation of the size distribution over time determined from log-normal parameterizations; not only is the the droplet mean diameter decreasing over time, but the distribution is also narrowing since the standard deviation shows a decrease over time. The rate of change in the droplet number and mass mean size will remain the focus of the discussion.

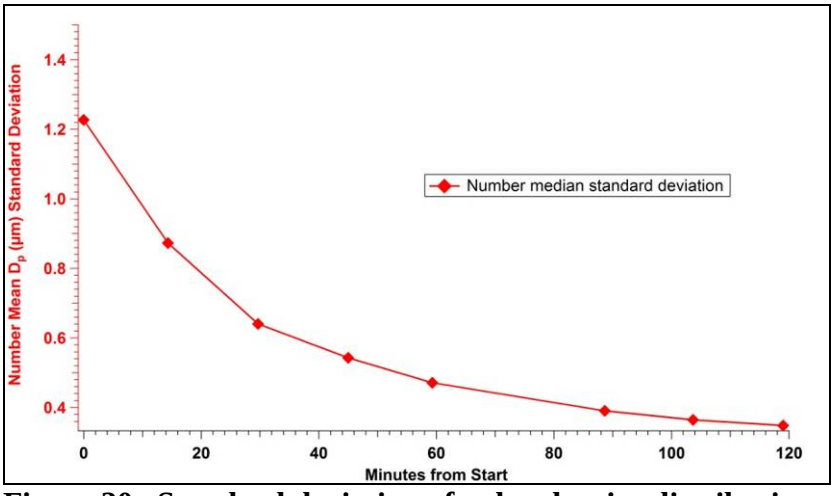

Figure 30. Standard deviation of a droplet size distribution over time

3.3.3. Aerosol Evaporation Rates – Charged vs. Uncharged Droplet Sprays

Figure 31 shows the median number and mass diameters over time for two DF-200 spray tests in which no voltage was applied using the ITW nozzle during dispersion. The number mean diameters of the initial spray distribution are between 1.5 µm and 2.0 µm and decrease to a median number diameter near 0.65 µm. Furthermore, each rate of decrease was fit using an exponential of the form:

$$D_p(\mu m) = D_{p0}(\mu m) + A \exp\left(\frac{t}{\tau}\right)$$

where τ refers to the *e*-folding rate of decrease in droplet diameter (the rate at which the droplet diameter will be *~2.72* times less than the originally injected diameter). The mass mean diameter, which represents the median of the log-normal fit for the size resolved volume distribution, is plotted in blue and has an initial value near 5 µm and an ending diameter near 1.5 µm. With the exception of the initial measurement, the ratio of the mass mean diameter to the number mean diameter remains constant at a value near 1.6. The particle population also exhibits a rate of decrease in droplet diameter (τ) between 30 and 35 minutes. Therefore, given a liquid dispersion of DF-200 droplets using the ITW nozzle under the experimental parameters listed above and zero charge applied to the droplets upon dispersion, the droplet diameter is expected to decrease in size by a factor of *e* in approximately 35 minutes. For both of the cases presented in Figure 31, the relative humidity remained below 60%.

Figure 32 shows the results for the size distribution analysis over time for a DF-200 droplet dispersion with a voltage of 3 kV applied to the ITW Rotary Atomizer apparatus. This results in a charged spray distribution within the mixing chamber. Under these conditions, the initial drop size remains consistent with the no-charge case in which the number median diameter is between 1.5 µm and 2.0 µm. However, the ending particle diameter is around 0.5 µm. The mass mean diameter under these conditions decreases to roughly 0.5 µm (also consistent with the zero voltage case) to around 1.2 µm, but does so at a visibly faster rate. Furthermore, the ratio of mass to number median diameter varies throughout the measurement period but remains consistently above 1.7 with the majority of the ratios above 2.2. In addition, when a voltage of only 3 kV is applied to the DF-200 dispersion spray, the *e*-folding rate of change in particle size decreases from around 35 minutes to around 25 minutes as shown by the fit rate (orange dashed line) in Figure 32, where each experiment was exposed to an environmental relative humidity below 60%.

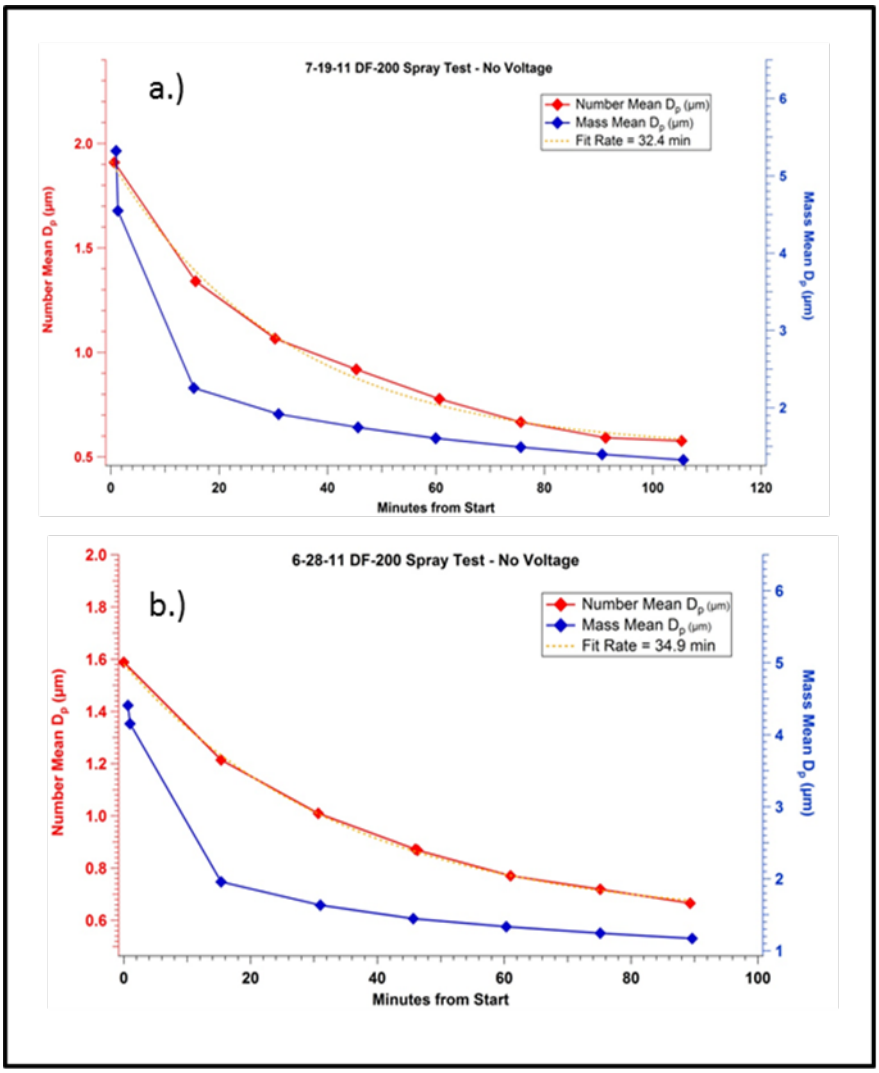

Figure 31. Number and mass mean diameter for a DF-200 droplet population with no voltage applied to the spray dispersion

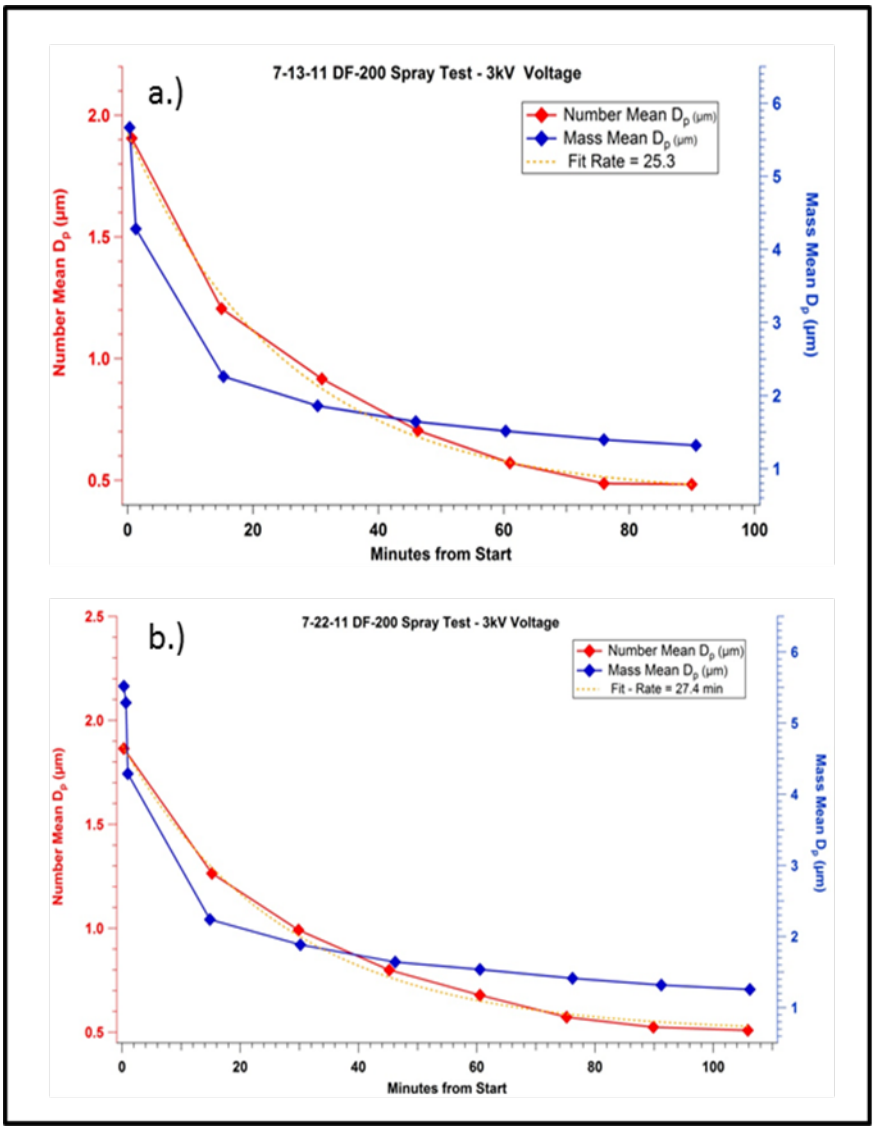

Figure 32. Number and mass mean diameter for a DF-200 droplet population over time with a 3 kV voltage applied

3.3.3.1. Low vs. High Relative Humidity

DF-200 aerosolized droplets were dispersed using the ITW nozzle under both dry and humid environmental conditions with a chamber temperature controlled to near 73ºF. For the purposes of this study, a dry environmental condition refers to a relative humidity that remains below 65%. In conjunction with the classical theory of evaporation as detailed in Section 3.1, a 65% relative humidity falls on the middle leg of the hysteresis curve for a salt-solution droplet. The only increase in relative humidity within the environmental mixing chamber is due to the evaporation of DF-200 droplets. For the low relative humidity case, the ITW nozzle was used to disperse the solution droplets only until the concentration within the chamber reached 10^4 particles/cm^3. This conditional generation was sufficient to ensure that the relative humidity within the chamber did not reach over 65%. Figure 33 shows the median number and mass droplet diameters for two separate low humidity tests. The relative humidity data is plotted in green.

The initial number median diameter recorded on 7-19-2011 (Figure 33a.) was 1.9 µm. Following initial dispersion, the droplet diameter decreases exponentially to an ending diameter near 0.6 µm with an *e*-folding timescale equal to 32.4 minutes. Similarly, an initial median diameter near 1.5 µm was recorded on 6-23-11 (Figure 33b.) decreasing to near 0.5 µm with an exponential decay timescale of 31.4 minutes. In each case, the ending diameter was 3 times smaller than the initially injected diameter with a beginning relative humidity near 55%. Comparing these results to what is expected for a pure NaCl salt solution droplet; a pure salt solution droplet would decrease in size close to 2.0 times its originally injected diameter assuming a solution droplet was generated under >95% relative humidity.

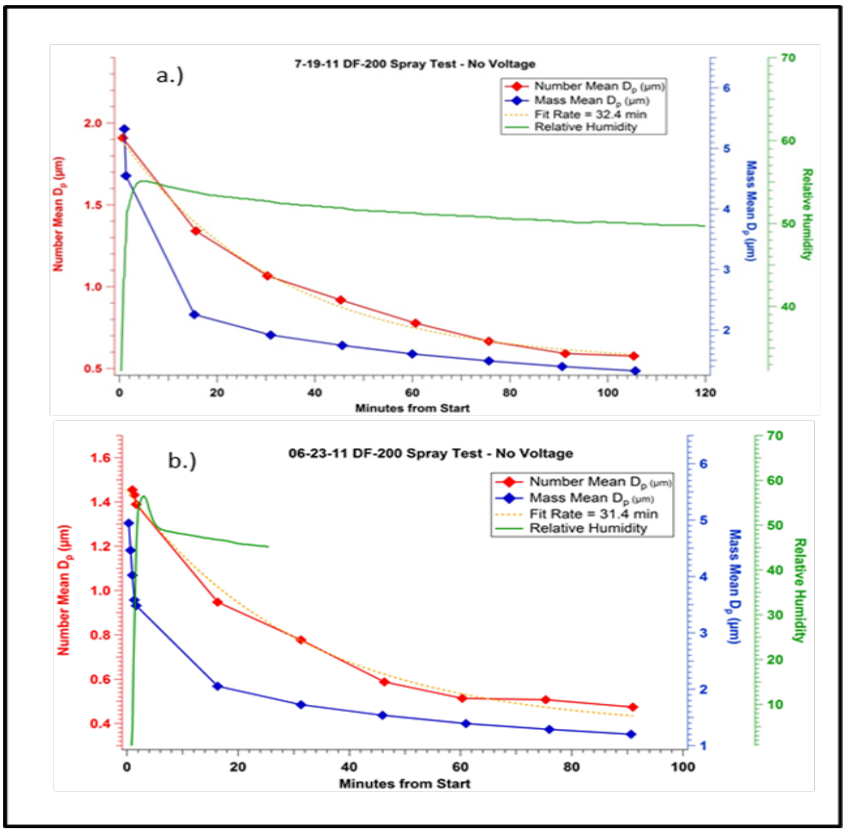

Figure 33. Number and mass mean diameter for a low relative humidity (green) condition

Figure 34 shows the resulting median diameters for DF-200 droplets under humid conditions. Here, we will consider a humid condition to be at or above 85% relative humidity. In order to reach a relative humidity of 85%, the ITW nozzle was used to spray aerosolized DF-200 into the chamber until the target of 85%. Because of the high water content in the DF-200 droplets, the target relative humidity generally took less than 10 minutes to reach. Once 85% was recorded by the RH probe, aerosol generation was ceased, and the chamber was sealed from room air.

The initial droplet diameters for each experiment plotted below are near 0.95 µm with mass median diameters near 4.5 µm. For both experimental cases presented, the ending diameter occurs at a relative humidity near 87% with a value of 0.5 µm and an exponential decay rate of ~45 minutes. The ending mass median diameter recorded for each test was 0.97 µm. For the high humidity condition, the ratio of the beginning to ending droplet diameter is equal to 2.0 at

87% relative humidity whereas a pure salt solution droplet would only decrease in size by a factor of 1.3. Not only does a higher humidity environment preserve the droplet over longer timescales, but the overall loss of material from the droplet is lower than under the low humidity experimental condition in agreement with experimental results of solution droplet hysteresis. Further studies investigating the evaporation characteristics of DF-200 droplets under extreme environmental conditions would broaden the applicability of these results.

Figure 35 shows the decrease in median diameter and subsequent increase in relative humidity for DF-200 droplets plotted against the relative humidity measured for a pure water dispersion tests. Of particular note is that the relative humidity conditions for DF-200 droplets do not exceed 87% on either test date while the relative humidity for pure water increases to near 95%. This result is consistent with theoretical predictions for the evaporation of solution droplets discussed in Section 3.1 and provides evidence supporting Raoult's Law; the saturation vapor pressure at the surface of a pure water droplet is higher than that for a DF-200 droplet under identical dispersion conditions.

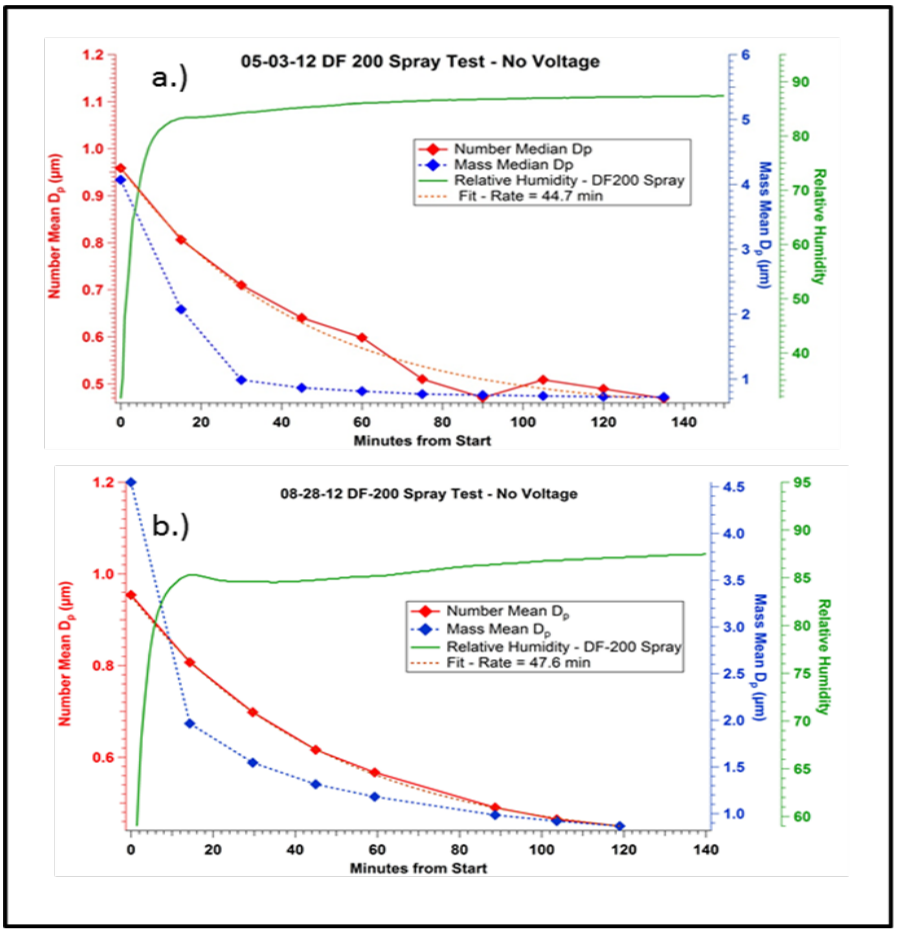

Figure 34. Number and mass mean diameter for a high (green) relative humidity condition

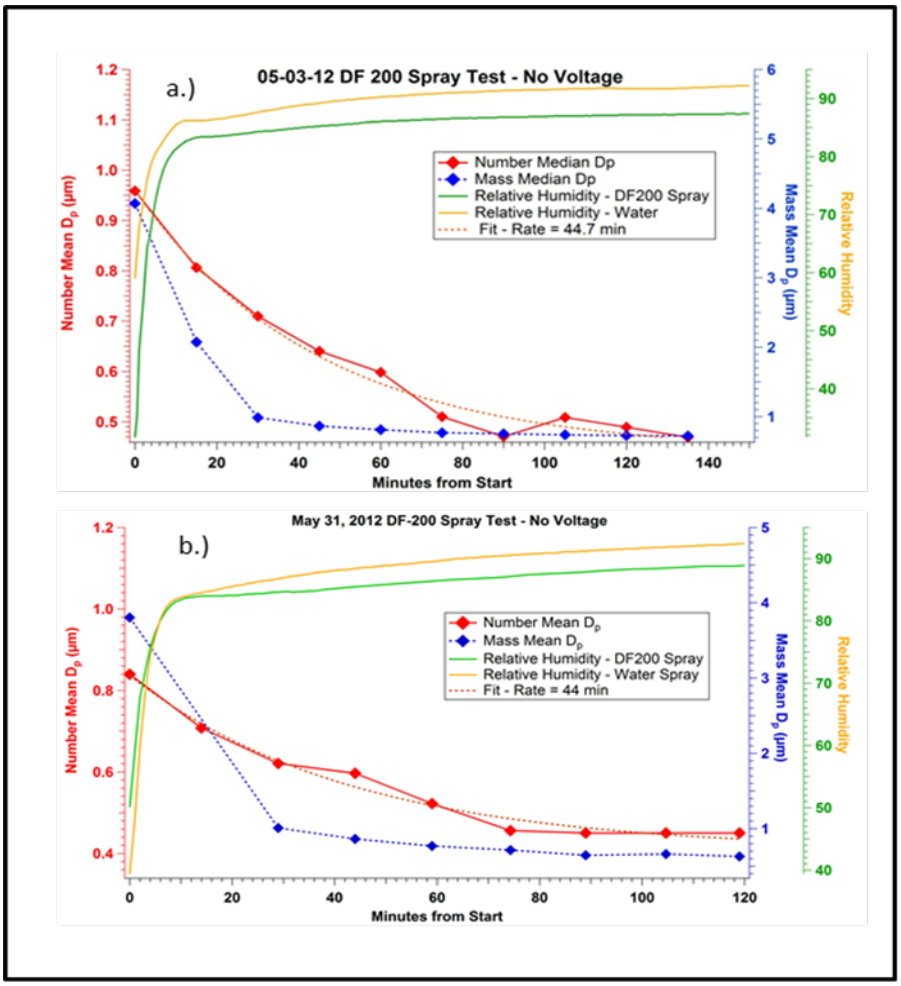

Figure 35. Number and mass mean diameter for a high relative humidity (green) condition compared to the relative humidity for pure water droplet dispersion (orange)

3.3.4. Droplet Chemistry Characterization and Analysis

The concentrations of two DF-200 constituents, diethylene glycol monobutyl ether (DEGMBE) and 1-dodecanol, were determined by GC/MS analysis of the iso-octane extraction solution, following extraction of the aerosol particles collected on glass fiber filters. The concentrations of DEGMBE and dodecanol in DF-200 are 0.78 and 0.39% by weight (based on the Sandia preferred formulation, and not necessarily on the manufacturer's final blend), respectively, a ratio of nearly 2:1. As measured by GC/MS analyses, the ratios of DEGMBE concentration to dodecanol concentration measured in the aerosolized droplets did not match the actual weight % ratio in DF-200, and the measured DEGMBE:dodecanol ratio was not consistent from test to test. The test environmental conditions (RH, temperature) remained relatively consistent within sampling points of a test series ($\pm$ ~3%) and are not presumed to be the cause of the inconsistencies in the measured concentrations of the two co-solvents. I.e., any changes in aerosol concentrations due solely to variance in vapor pressures between the two components would have followed a similar trend as the environmental parameters were maintained within a test series. As discussed in Section 3.2.2, the sampling frequencies and duration remained constant across all tests. The vapor pressure of DEGMBE is 0.01 mm Hg at 25°C; the vapor

pressure of 1-dodecanol is 0.002 mm Hg at 25°C. Due to a combination of evaporative and depositional particle losses and the lower vapor pressure of dodecanol, one would expect the aerosol concentration of dodecanol to decrease at a much *slower* rate than DEGMBE, thereby approaching a 1:1 aerosolized ratio over time. The results indicate the ratio of these components in the aerosolized droplets measured at any given time point to be approximately 1:1, DEGMBE:dodecanol. That the measured ratio is approximately 1:1 at the initial sampling is unexpected and cannot be explained. As DF-200 is a mixed reactive solution, the impact and dynamics of the combined constituents on overall droplet evaporation is clearly evident and influential. Results also suggest that the GC/MS method and/or system parameters be re-examined for optimal performance.

Representative results of tests performed on April 5, April 12 and April 26 are displayed in Figure 36. The goals of this test series were to use the ITW-generated DF-200 spray to reach the high RH condition, ~ 85%, and monitor particle rate losses and chemistry in the high RH condition. The DEGMBE and dodecanol concentrations measured from the second filter extract (Sample 2, collected 15 minutes from the start of the test) were the highest of the three filter samples; this trend in inconsistent with what would be expected, based on the consistent observation of decreasing aerosol particle density over the test duration. The DEGMBE and 1-dodecanol concentrations should have been highest when the APS total particle density peaked at the Sample 1 time point. As shown in all figures of Section 3.3.3, the mass mean and number mean aerosol particle diameters are decreasing at consecutive sampling time points. However, the decreases in DEGMBE and 1-dodecanol concentrations from the second to the third filters do follow the expected trend as a result of evaporative particle losses.

Figure 36. Representative concentrations of DEGMBE, dodecanol (by GC/MS) and total particles by APS in aerosolized DF-200 sprays

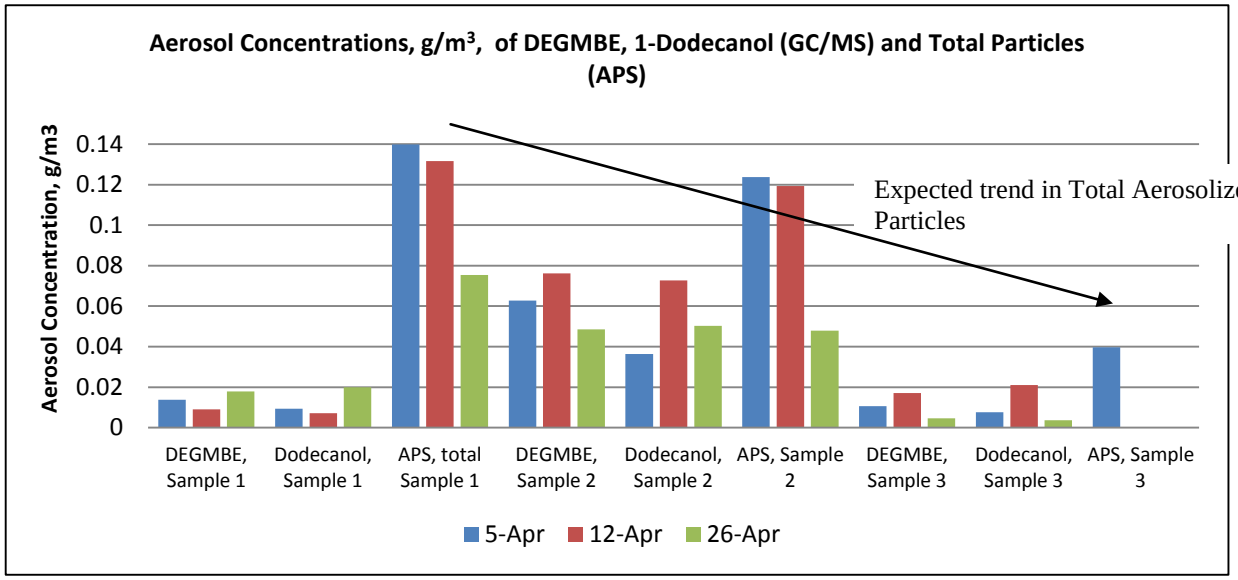

Inconsistencies in the ITW nozzle dispersion across time and the variations in measured concentrations of chemical constituents reduce the ability to make conclusive statements regarding the chemical composition with reasonable confidence. As indicated in Figure 37, the decrease in total aerosol population (mirrored by similar trends in decreased DEGMBE and dodecanol aerosol concentrations) from the April to May timeframe could be indicative of a reduced ITW nozzle performance. The nozzle was specially fabricated for a previous project, and has been utilized inconsistently over a period of approximately 5 years. Maintenance and refurbishment was performed by the manufacturer between June through early August. Upon return to operation in August, the particle distribution was reported to have increased approximately 1 order of magnitude across the lower end of the distribution curve (< 1 micron), although as shown in Figure 37, there was a noticeable decrease in the *total* aerosolized population when compared to tests performed in April, prior to refurbishment. Note that the goals of the May tests were to reach a RH of ~ 82-83%, and the goals of the August test series were to reach 83-85% RH.

Figure 37. The Concentrations of DEGMBE, 1-Dodecanol and total particles in aerosolized DF-200.

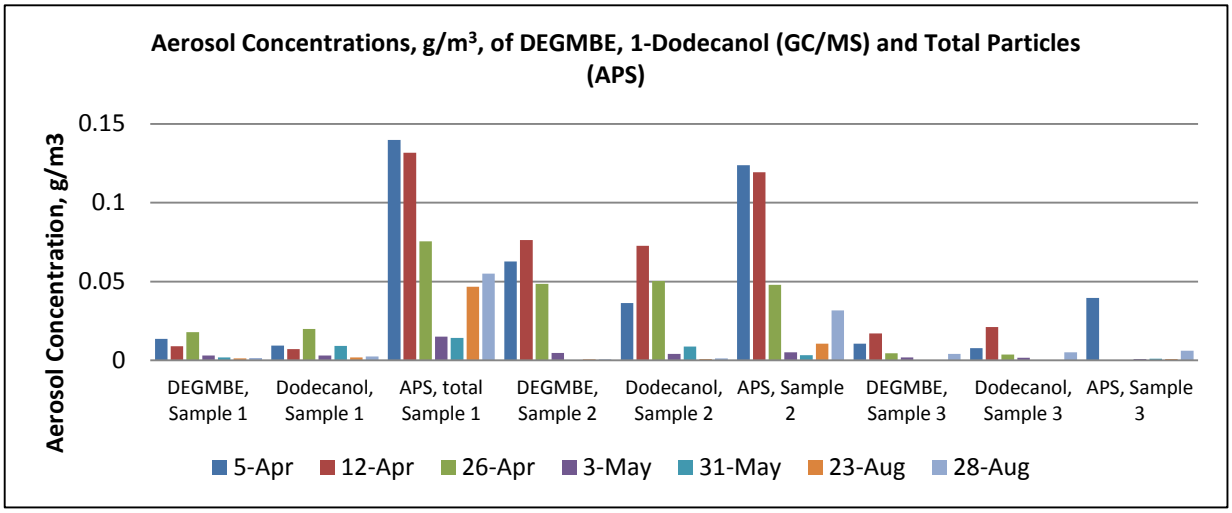

3.4. Conclusions – DF-200 Aerosolized Droplet Characterization

For a limited set of ITW conditions (3 kV, 30K rpm), exponential rate losses were determined to be 30 and 45 minutes, respectively, for dry and high RH chamber environments. The sampling efficiency of aerosolized chemicals by SKC BioSampler devices was demonstrated to be comparable to aerosol concentrations as determined by the APS. The averaged concentration of oleic acid measured from both the APS and the SKC BioSampler collection fluid was within an order of magnitude. As aerosolized chemical simulant species are typically dispersed at concentrations 6 to 7 orders of magnitude greater than GC/FPD or GC/MSD detection limits, it can be concluded that the SKC collection efficiency of aerosolized chemical species are within a reasonable range, given experimental error within the test procedure from sampling line depositional losses, evaporative losses during sampling, or errors in weighing or the analytical process.

The project did not accomplish the full set of objectives originally proposed in the aerosol test plan, partly due to the fact that the GC siloxane-based columns degrade upon extended exposure to an aqueous phase and are therefore not appropriate for the direct analysis of vapor-phase aqueous solutions such as DF-200. This precluded the use of direct sampling lines to the GC/MSD detector for the analysis of vapor phase constituents and the analysis of transport from aerosol particle evaporative losses to the vapor phase. Thus, one of the primary recommended improvements for future efforts is to use direct sampling and analysis techniques for analyses of chemical constituents in both aerosol and vapor phases. Use of direct sampling and analysis techniques should also improve the precision of chemical composition measurements.

Additional recommendations for future projects with similar goals include the use of better methods for quantification of small particle distributions, especially those < 500 nm; use of the Malvern Particle Size Analyzer for analysis of the full droplet distribution; and construction of a seamless Teflon chamber that is more resistant to chemical permeation. Importantly, the operational integrity and performance of the ITW nozzle should be verified prior to start of a long-term research project. Routine maintenance of the titanium cup requires daily sonication and thorough rinsing.

4. CONCLUSIONS AND PROPOSED NEXT STEPS

Broadly speaking, one of the more valuable lessons learned throughout the project was an altered rationale for approaching decontamination development in the future. This change in approach was developed through observations and results from this project, as well as those from a project being performed coincidentally. The proposed effort for this LDRD was focused on gaining solution based micellar characterization. From an applied sense, a more critical need is to improve the removal and neutralization of CBW agents or other toxins that are bound or adsorbed to surface matrices. Thus, understanding the associated transport issues as reactive chemistries are applied onto contaminated surfaces should be the initial directive for a project targeting improvements to decontamination efficacy. The transport of chemical species is altered by surface chemistry, reaction dynamics and other environmental factors. A thorough analysis or characterization of select material matrices, and the mechanisms and relational positioning of critical atoms as agents or simulant become absorbed and adsorbed within materials becomes primary. The presence of water or other reactive species (e.g., cationic binding sites or reactive hydroxyl species inherent to concretes) is a key element impacting the dynamics of surface decontamination. The presence of environmentally inherent soils or other organic loads on surfaces is an element that has not been fully evaluated under many programs focused on either development, or test and evaluation of decontamination technologies. Efficacy testing should include in-situ monitoring of contaminants and decontaminants applied on surfaces representative (inherently soiled) of scenario defined conditions. Transport modeling may also be useful if relatively well-defined surface compositions are available.

The use of NMR partitioning studies may be especially useful to inform the cause and effect as individual components are added to form a reactive mixture. These effects could be compared to agent or simulant kinetic results to rationalize compositions that produce favorable kinetics and/or surface decontamination performance. The use of NMR should be most useful in comparing solutions that are highly reactive in solutions versus those that are highly efficacious on surfaces, as the two are not always congruent. Interesting topics for future efforts in this area include the following: 1) Monitoring the micellar environment following the addition of CBW simulants; 2) Studies utilizing a range of non-ionic, cationic or anionic surfactants; and 3) It is unknown what physical changes occur in the micelle system by the formation of oxidative species such as hydroxide (OH^-), hydroperoxicarbonate (HCO_4^-), and the hydroperoxide anion (OOH^-) following addition of peroxide. Time-dependent changes in the micelle characteristics could be compared to neutralization rates to determine in-situ rate limiting processes.

Once correlated to both simulant and live agent performance data (both solution kinetics and surface decontamination efficacy), it is anticipated that micelle characterization data will be useful to rationalize optimal conditions and thus formulation design. Understanding the changes that occur will be used to optimize the decontamination process, thus enhancing efficacy of various deployment modes.

The variation of ITW nozzle parameters originally proposed under this LDRD project is being studied, and methods for deployment are being developed under another ongoing project. Therefore, the advancement of the ITW rotary atomized CBW decontamination technique and methods for deployment continue at Sandia National Laboratories.

5. IMPACT OF THE PROJECT

The overall impact of this work was to foster a re-direction of approach in the development of decontaminants towards scenario relevant, in-situ evaluations. The insight gained from this project will allow for the more rapid evolution and optimization of decontamination formulations and applications. The re-directed approach will improve the efficiency at which the technical challenges are addressed during the development and performance assessment of decontaminants. It is anticipated that newer approaches will improve the ability to respond to surface decontamination inefficiencies.

Internally, the DSA and IHNS SMU's have benefitted from this project by significant improvements to Sandia's CBW response capabilities, effective in a wider variety of release scenarios. Sandia is now in a more valuable position to respond to new decontamination opportunities at DHS and other agencies. The timeframe for future success is 1 – 3+ years.

The work will be shared with our current DHS sponsor, with opportunity to network with DTRA PMs and other agencies by attendance and presentations at conferences. This work has helped to maintain Sandia as the government's lead expertise in decontamination technology development and application.

6. REFERENCES

Aswal, Vinod, *Small-Angle Scattering from Micellar Solutions,* BARC Newsletter available at www.barc.ernet.in/publications/nl/2003/200310-4.pdf.

Bahri, M.A., Hoebeke, M., Grammenos, A., Delanaye, L., Vandewalle N., and Seret A., *Investigation of SDS, DTAB and DTAB Micelle Microviscosities by Electron Spin Resonance*, Colloids and Surfaces A: Physicochem. Eng. Aspects 290 (2006) 206–212.

Betty, R.G.., Lucero, D.A., Brockmann, J., Tucker, M.D., Leonard, J., Wilson, W., Servantes, B., Sanchez, A., Allen, A., and Tezak, M., *Release Mitigation Spray Safety Systems for Chemical Demilitarization Applications (OUO)* SAND2010-4023, Sandia National Laboratories, Albuquerque, NM, June 2010.

Gharibi, H., Javadian, S., Sohrabi, B., and Behjatmanesh, R., *Investigation of interaction parameters in mixed micelle using pulsed filed gradient NMR spectroscopy*, Journal of Colloid and Interface Science 285 (2005) 351-359.

Hickok, R.S., Wedge, S.A., Hansen, A.L., Morris, K.F., Billiot, F.H., and Warner, I.M., *Pulsed field gradient NMR investigation of solubilization equilibria in amino acid and dipeptide terminated micellar and polymeric surfactant solutions*, Magnetic Resonance in Chemistry, 2002, 40:755-761.

Ho, P., Tucker, M.D., and Smith, W., *Decontamination Technologies for Building Restoration (OUO),* SAND2006-6580, Sandia National Laboratories, Albuquerque, NM, October 2006.

Joutsensaari, J; Vaattovaara, P; Vesterinen, M; Hameri, K; and Laaksonen, A (2001), *A novel tandem differential mobility analyzer with organic vapor treatment of aerosol particles*, Atmospheric Chemistry and Physics Vol. 1(1), 51-60.

Kulmala, M., Maso, M. D., Makela, J. M., Pirjola, L., Vakeva, M., Aalto, P., Miikkulainen, P., Hameri, K. and O'Dowd, C. D. (2001), *On the formation, growth and composition of nucleation mode particles*. Tellus B, 53: 479–490. doi: 10.1034/j.1600-0889.2001.530411.x.

Seinfeld, J. H. and Pandis, S. N.: *Atmospheric Chemistry and Physics: from Air Pollution to Climate Change*, John Wiley, New York, 1998.

Slinn, S.A., and Slinn, W.G.N, *Predictions for particle deposition on natural waters*, Atmospheric Environment (1967), Volume 14, Issue 9, 1980, Pages 1013-1016, ISSN 0004-6981, 10.1016/0004-6981(80)90032-3.
(http://www.sciencedirect.com/science/article/pii/0004698180900323)

Appendix A: ITW Aerosol Droplet Characterization Test Matrix

Test Date	Test Objective	ITW Spray Flow Rate (liquid, mL min)	ITW Fluid Pressure (psi)	ITW Flow Pressure (air, psi)	Turbine Speed (RPM)	ITW Shaping Air (CSFM)	Applied Voltage (kV)
06/9/11	Baseline Sampling	Not Recorded	32	42	30,000	100	0
06/10/11	DF-200 Baseline	Not Recorded	32	42	30,000	100	0
06/14/11	DF-200 Baseline	Not Recorded	32	42	30,000	100	0
06/22/11*	DF-200 Baseline	Not Recorded	32	42	30,000	100	0
06/23/11*	DF-200 Baseline	Not Recorded	31	42	30,000	100	0
06/28/11	DF-200 Baseline	Not Recorded	32	42	30,000	100	0
07/12/11*	DF-200 Baseline	~ 10	32	42	30,000	100	3
07/13/11*	DF-200 Baseline	~ 10	32	42	30,000	100	3
07/19/11	DF-200 Baseline	~9, 8.9	32	42	30,000	100	0
07/22/11	DF-200 Baseline	8	32	42	30,000	100	3
08/03/11	DF-200 Baseline	9.3, 9.8	32	42	30,000	100	3
08/04/11	DF-200 Baseline	9.5, 9.0	32	42	30,000	100	0
10/04/11		11	32	42	30,000	100	0
10/05/11		9	32	42	30,000	100	0
11/01/11	(3 in series) SKC Biosampler Collection Efficiency	10	3	16	30,000	100	0
11/08/11	(3 in series) SKC Biosampler Collection Efficiency	10	3	18	30,000	100	0
12/15/2011	(2 in series) SKC Biosampler Collection Efficiency	10	40	40	30,000	100	0

Test Date	Test Objective	ITW Spray Flow Rate (liquid, mL min)	ITW Fluid Pressure (psi)	ITW Flow Pressure (air, psi)	Turbine Speed (RPM)	ITW Shaping Air (CSFM)	Applied Voltage (kV)
1/26/2012	(2) SKC Biosampler Collection Efficiency	10	13	20	32,000	100	0
03/08/12	(1) SKC Biosampler Collection Efficiency	10	13	20	30,000	100	0
03/20/12	DF-200 Baseline	10	40	40	30,000	100	0
04/02/12*	TRH W/ DF-200	10			30,000	100	0
04/05/2012	TRH W/ DF-200	10	25	30	30,000	100	0
04/12/12*	TRH W/ DF-200	10	24	29	30,000	100	0
04/26/12*	TRH W/ DF-200	10	20	20	30,000	100	0
05/03/12*	TRH W/ DF-200	10	22	23	30,000	100	0
05/24/12	Water Baseline	10	23	22	30,000	100	0
05/31/12*	DF-200 Baseline	10	28	23	30,000	100	0
08/23/12*	DF-200 Baseline	10	7	21	30,000	100	0
08/28/12*	DF-200 Baseline	10	7	18	30,000	100	0

DISTRIBUTION OF ELECTRONIC COPIES

1	MS0734	Rita Betty	06632
1	MS0734	J. Bruce Kelley	06632
1	MS0734	Mark Kinnan	06632
1	MS0734	Gretchen Taggart	06632
1	MS0734	Mark Tucker	06632
1	MS0886	Todd Alam	01816
1	MS1135	Crystal Glen	01532
1	MS1135	Danielle Rivera	01532
1	MS1135	Andres Sanchez	01532
1	MS1135	Randy Watkins	01532
1	MS1349	Hongyou Fan	01815
1	MS9004	Duane Lindner	08120
1	MS0899	Technical Library	9536 *(electronic copy)*
1	MS0359	D. Chavez, LDRD Office	1911


Sandia National Laboratories